Modeling the rocking and sliding of free-standing objects using rigid-body dynamics

by Swetha Veeraraghavan, John F. Hall, and Swaminathan Krishnan

Abstract

A rigid body dynamics algorithm is presented in this paper to simulate the interaction between two rigid bodies in the presence of static and kinetic friction forces. Earlier algorithms led to different solutions when parameters external to problem description, such as ordering of contact points, are changed. This paper addresses the issue of selecting an appropriate solution for the contact forces and impulses from the infinite set of solutions by picking the solution that is closest to the previous state of the rigid body. The capability of this algorithm to simulate pure rocking, pure sliding and combined rocking and sliding response modes of a rectangular block is validated using analytical results. This validated algorithm is later used to identify the various response modes of a rectangular block which is given an initial tilt and then released.

Introduction

An object which can only translate and rotate and cannot deform is called a rigid body. Idealizing objects which undergo negligible deformation as rigid bodies has helped in simplifying and obtaining analytical solutions to many complex problems [12, 29, 31]. This usefulness of rigid body dynamics had led to the development of fast and robust algorithms for use in engineering [25, 26], computer graphics [2, 24] and robotics [10, 21].

In most rigid body dynamics algorithms, two disjointed rigid bodies are considered separately and the interaction between them is modeled using contact forces or impulses. There are two ways to compute these contact forces/impulses - the penalty stiffness method and the constraint based method. Baraff [1] provides a detailed comparison between these two methods. In the penalty stiffness method, which has many applications that involve deformable bodies, contact force is proportional to the distance one body interpenetrates the other [15]. This is analogous to modeling contact using a spring-damper assembly. The high spring stiffness required for realistic (low inter-penetration) simulation can lead to instabilities and increase the cost of simulation. The penalty stiffness method works well when modeling the contact between a rigid and a deformable body. There has been some recent research on the response of 2D and 3D rectangular blocks on a deformable base subjected to earthquake excitation using the penalty stiffness method [6, 7].

In the constraint based method, the forces/impulses are calculated such that non-penetration constraints between the rigid bodies are satisfied. There are two ways of achieving this - (i) using impulses alone, (ii) using impulses as well as contact forces. In the first approach [3, 4, 30], impulses are applied at points where two rigid bodies collide. These impulses are calculated such that the rigid bodies are either touching each other (relative normal velocity is zero) or moving away from each other (relative normal velocity is positive) at the contact points after the collision. In between collisions, each rigid body is assumed to be under free flight, i.e., the presence of other rigid bodies are not acknowledged. This method is useful for the dynamic simulation of cluttered environments where rigid bodies collide often. However, it is not efficient for simulating scenarios with sustained contact like books stacked on a book-shelf.

In the second approach, impulses are applied to satisfy velocity constraints (similar to the first approach), and if the contact persists, then contact forces are applied to prevent rigid bodies from accelerating towards each other at the contact points. This approach addresses the issue of rigid bodies in sustained contact but is not efficient in simulating large number of rigid bodies colliding with each other due to the additional expense of computing contact forces. Lötstedt [20] was the first to handle contacts in this way. Baraff [2] presented a fast algorithm based on Cottle and Dantzig's algorithm [8] to compute the contact forces and impulses efficiently.

Each of the methods described above are crafted for problems of a specific type. The focus of this paper is on simulating response of free-standing rigid objects like stone columns/statues or precariously balanced rocks to ground excitation. Here, the rigid block is one rigid body and the ground is another rigid body but with infinite mass and moment of inertia. Initially, the rigid block is sitting on the ground and the contact between them is maintained for varying periods of time depending on the acceleration of the ground. Therefore, the constraint based method using both impulses as well as contact forces is the best way to approach this problem. The problem set up is similar to the one formulated by Baraff [2].

The contact forces play an important role in determining the total acceleration of the block at any instant in time. In Baraff's algorithm, the problem of computing contact forces (normal and frictional contact forces) is posed as an optimization problem. Due to the ill-constrained nature of the optimization problem, it can result in infinite solutions for the contact forces. In certain cases (e.g., friction-less systems), all the contact force solutions lead to the same total acceleration of the rigid body. However, in the presence of static friction forces satisfying Coulomb friction law, all the solutions may not result in the same total acceleration.

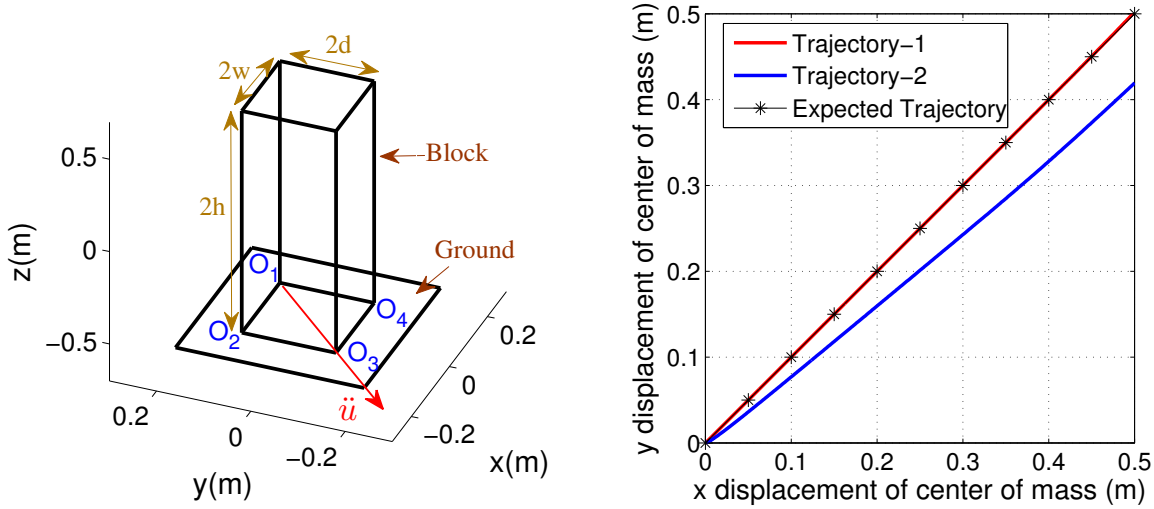

(a) (b)

Figure 1: (a) Rigid cuboid sitting on rigid ground accelerating with horizontal acceleration $\ddot{u}$; (b) Expected horizontal trajectory of the center of mass of the block and two trajectories obtained from implementation of Baraff's algorithm. Trajectory-1, which matches with the expected trajectory, is obtained when contact force calculation starts with point O_1, and trajectory-2 is obtained when the contact force calculation starts with point O_2.

For example, let us consider the case where a rigid square cuboid of mass $m = 100$ kg with half width $w = 0.1$ m, half height $h = 0.6$ m and half depth $d = 0.1$ m is resting on a rigid horizontal ground [Fig. 1(a)]. Say the cuboid comes in contact with the ground at only the four corners (O_1, O_2, O_3 and O_4). If gravity g is the only external acceleration on the cuboid, the contact forces at all corners can be equal (i.e., $mg/4$) or the forces at opposite corners can be equal, (i.e., $O_1 = O_3$, $O_2 = O_4$) such that O_1 and O_2 are

positive real numbers satisfying $O_1 + O_2 = mg/2$. So, there are infinite combinations of forces that result in zero total translational and rotational acceleration of the cuboid, i.e., the cuboid will remain at rest. In addition to gravity, if the ground constantly accelerates along the diagonal direction opposite to O_1 with a magnitude $\ddot{u}$, which is greater than the quasi-static toppling acceleration of the cuboid (i.e., the minimum constant ground acceleration required for the cuboid to overturn), then it is expected that the block will rotate about the corner O_1 and overturn. For a static friction coefficient $\mu = 1.2$, which is sufficiently high to prevent sliding between the cuboid and the ground, Baraff's algorithm results in two possible dynamic paths for the cuboid [Fig. 1(b)]. For clarity, only the plan (x-y plane) projection of the displacement of the center of mass relative to the ground is presented. The line with the asterisk markers is the expected trajectory which is the $x = y$ line due to the symmetry in the geometry of the cuboid and the applied ground acceleration.

Baraff's algorithm is an iterative procedure in which the forces at the contact points are handled sequentially. Say the algorithm starts at corner O_1, the normal contact force for point O_1 is calculated such that the normal contact constraints are satisfied for this contact point. Then, the friction force in X-direction is calculated followed by the friction force in Y-direction such that the friction constraints are satisfied. During the calculation of the friction forces, the normal force is altered so that the normal contact constraints continue to hold. This is repeated for the next contact point O_2 making sure the normal and frictional constraints for point O_1 are still satisfied. The algorithm terminates when the normal and friction constraints are satisfied at all contact points. This can happen after calculating forces for just corner O_1 or corners O_1 and O_2 etc. Due to the sequential treatment of the contact points, this algorithm leads to different solutions based on the order in which the contact points are considered or the order in which the friction forces are calculated (X direction followed by Y direction). For the above example, if the algorithm starts with contact point O_1, then it results in trajectory-1 but if O_2 is considered first, then it leads to trajectory-2 [Fig. 1(b)]. Both solutions are permissible and mathematically correct. However, the deviation of trajectory-2 from the expected trajectory, caused by artificial twisting of the block about the vertical axis, violates the inherent symmetry of the problem.

Baraff's algorithm is aimed at obtaining fast simulations for computer graphics and robotics applications for which this iterative algorithm works well. It is the de-facto standard algorithm used in simulation software packages such as Maya and Open dynamics engine [23]. Past works on this topic have focused solely on solving the optimization problem without due regard to solution selection consistent with the physics of the problem (from the infinite set of solutions). In this paper, an alternate method to solve the optimization problem formulated by Lötstedt and Baraff is presented. The main idea behind this algorithm is that at each dynamic time step the rigid body will choose the contact force solution that is closest to the equilibrium state of the rigid body at the previous time step. This will always lead to the symmetric solution [e.g., trajectory-1 in Fig. 1(b)] if one is present. Here, we outline the rigid body dynamics algorithm, validate it with analytical results for the rocking and the coupled sliding-rocking response of a rectangular block, and apply it predict all response modes of a rectangular block.

Rigid body dynamics algorithm

Consider a rigid body rotating and translating in space. Let $\mathbf{u_{cm}}(t)$ and $\dot{\mathbf{u}}_{\mathbf{cm}}(t)$ be the position vector and the translational velocity vector, respectively, of the center of mass (cm) in the global coordinate system, $\mathbf{R}(t)$ be the rotation matrix between the local and global coordinate systems which are initially co-located at the cm, and $\mathbf{l}(t)$ be the angular momentum of the rigid body about the cm in global coordinate system, all at time t. These four quantities are the state variables as they provide complete information about the rigid body at any instant in time. In this paper, bold lowercase letters are vectors and bold uppercase letters are matrices. All vectors and matrices are in the global coordinate system unless noted otherwise. The rate of

change of these state variables with respect to time are given by:

$$\frac{d}{dt}\mathbf{u_{cm}}(t) = \dot{\mathbf{u}}_{\mathbf{cm}}(t) \tag{1}$$

$$\frac{d}{dt}\dot{\mathbf{u}}_{\mathbf{cm}}(t) = \frac{\mathbf{f_T}(t)}{m} \tag{2}$$

$$\frac{d}{dt}\mathbf{R}(t) = \boldsymbol{\omega}(t) \times \mathbf{R}(t) \tag{3}$$

$$\frac{d}{dt}\mathbf{l}(t) = \boldsymbol{\tau_T}(t) \tag{4}$$

Here, $\omega(t)$ is the angular velocity [$\boldsymbol{\omega}(t) = \mathbf{I}^{-1}(t)\mathbf{l}(t)$], $\mathbf{I}(t)$ is the moment of inertia, $\mathbf{f_T}(t)$ is the net force, $\boldsymbol{\tau_T}(t)$ is the net torque about cm, and m is the mass of the rigid body. The moment of inertia at time t, $\mathbf{I}(t)$, can be calculated if its value at $t = 0$ is known [$\mathbf{I}(t) = \mathbf{R}^T(t)\mathbf{I}(0)\mathbf{R}(t)$].

The discussion above is for a general rigid body. We are interested in modeling the interaction between a rigid block and its the pedestal, a rigid body which does not rotate. The block and the pedestal are modeled separately with four state variables each. Let $\mathbf{u_{cm}}(t)$, $\dot{\mathbf{u}}_{\mathbf{cm}}(t)$, $\mathbf{R}(t)$ and $\mathbf{l}(t)$ be the state variables for the block and $\mathbf{u_p}(t)$, $\dot{\mathbf{u}}_{\mathbf{p}}(t)$, $\mathbf{R_p}(t)$ and $\mathbf{l_p}(t)$ be the state variables for the pedestal. Since the pedestal can only translate, the rotation matrix of the pedestal, $\mathbf{R_p}(t)$, is always the identity matrix and angular momentum of the pedestal, $\mathbf{l_p}(t)$, is always zero.

The aim of the algorithm is to obtain the state variables for the block and pedestal at time $t + \Delta t$ given the state of the system at time t. Since the pedestal has an infinite mass and moment of inertia, the contact forces and impulses resulting from the interaction of the pedestal with the block have no effect on the dynamics of the pedestal. Let $\ddot{\mathbf{u}}_{\mathbf{p}}(t)$ be the applied pedestal acceleration as a function of time. Then, pedestal displacement and velocity at $t + \Delta t$ may be determined by time-integrating Eqs. 1 and 2 using the constant average acceleration method:

$$\mathbf{u_p}(t + \Delta t) = \mathbf{u_p}(t) + \frac{\Delta t}{2}[\dot{\mathbf{u}}_{\mathbf{p}}(t) + \dot{\mathbf{u}}_{\mathbf{p}}(t + \Delta t)] \tag{5}$$

$$\dot{\mathbf{u}}_{\mathbf{p}}(t + \Delta t) = \dot{\mathbf{u}}_{\mathbf{p}}(t) + \frac{\Delta t}{2}[\ddot{\mathbf{u}}_{\mathbf{p}}(t) + \ddot{\mathbf{u}}_{\mathbf{p}}(t + \Delta t)] \tag{6}$$

However, obtaining the state variables for the block at $t + \Delta t$ is not as simple. The state variables have to be estimated iteratively so that the block is in dynamic equilibrium at $t + \Delta t$. The outline of the algorithm is shown in Algorithm 1.

The following are the steps to go from time-step iteration k to iteration $k + 1$ (outermost while loop) for the state variables of the block.

Step 1: Integrate differential equations.

To estimate the state variables of the block at $t + \Delta t$, the differential Eqs. 1 - 4 for the block are time integrated using constant average acceleration method to yield:

$$\mathbf{u_{cm}}^{k+1}(t + \Delta t) = \mathbf{u_{cm}}(t) + \frac{\Delta t}{2}[\dot{\mathbf{u}}_{\mathbf{cm}}(t) + \dot{\mathbf{u}}^k_{\mathbf{cm}}(t + \Delta t)] \tag{7}$$

$$\dot{\mathbf{u}}^{k+1}_{\mathbf{cm}}(t + \Delta t) = \dot{\mathbf{u}}_{\mathbf{cm}}(t) + \frac{\Delta t}{2}\left[\frac{\mathbf{f_T}(t)}{m} + \frac{\mathbf{f_T}^k(t + \Delta t)}{m}\right] \tag{8}$$

$$\mathbf{R}^{k+1}(t + \Delta t) = \mathbf{R}(t) + \frac{\Delta t}{2}[\boldsymbol{\omega}(t) \times \mathbf{R}(t) + \boldsymbol{\omega}^k(t + \Delta t) \times \mathbf{R}^k(t + \Delta t)] \tag{9}$$

$$\mathbf{l}^{k+1}(t + \Delta t) = \mathbf{l}(t) + \frac{\Delta t}{2}[\boldsymbol{\tau_T}(t) + \boldsymbol{\tau_T}^k(t + \Delta t)] \tag{10}$$

$\mathbf{R}^{k+1}(t + \Delta t)$ is a rotation matrix, so its determinant should be unity and its inverse should equal its transpose. If these properties are not satisfied by $\mathbf{R}^{k+1}(t + \Delta t)$, Cayley transform [5] is used to project the

Algorithm 1 Rigid body dynamics algorithm

Input: block state variables at t, pedestal state variables at t and $t + \Delta t$
Output: block state variables at $t + \Delta t$

```
initialization
while block state variables at t + Δt not converged do
    update state variables at t + Δt using Eqs. 7 - 10      // Step 1
    if block penetrates the pedestal then      // Step 2
        reduce Δt
        go back to initialization
    end if
    if block and pedestal in contact then
        estimate impulses to resolve collision      // Step 3
        while normal impulses not converged do
            update normal impulses      // Step 3(a)
            update frictional impulses      // Step 3(b)
        end while
        estimate contact forces      // Step 4
        while normal forces not converged do
            update normal forces      // Step 4(a)
            update frictional forces      // Step 4(b)
        end while
    else
        no contact forces
    end if
end while
```

matrix back onto the admissible space of rotation matrices. If the block is initially at rest on the pedestal, then $\mathbf{u_{cm}}(0) = \mathbf{0}$, $\dot{\mathbf{u}}_{\mathbf{cm}}(0) = \mathbf{0}$, $\mathbf{R}(0) = \mathbf{I}$, the identity matrix, $\mathbf{l}(0) = \mathbf{0}$, $\mathbf{f_T}(0) = \mathbf{0}$, $\boldsymbol{\tau_T}(0) = \mathbf{0}$ and $\boldsymbol{\omega}(0) = \mathbf{0}$.

Step 2: Find contact points.

Using the state variables obtained in **Step 1**, the positions of the points on the outer surface of the block are updated. For example, if α is a point on the block and $\boldsymbol{r_\alpha}(0)$ is its initial position with respect to the cm, then, its updated position vector is:

$$\boldsymbol{u_\alpha}^{k+1}(t + \Delta t) = \mathbf{u_{cm}}^{k+1}(t + \Delta t) + \mathbf{R}^{k+1}(t + \Delta t)\boldsymbol{r_\alpha}(0) \tag{11}$$

Similarly, the positions of points on the pedestal surface are updated. At $t + \Delta t$, if any point of the block is within ϵ (tolerance) from the surface of the pedestal, then that point is assumed to be a contact point. However, if any point on the block's surface penetrates a distance more than ϵ into the pedestal, then the system is taken back to an earlier time t_c ($t \leq t_c \leq t + \Delta t$) when no point has penetrated more than ϵ into the surface of the pedestal and the calculations are carried out for the reduced time step.

With no point on the block's surface penetrating into the pedestal, we look for block points that are in contact with the pedestal. If none exist, it implies that the block is in free-fall under the action of gravity and the contact forces are set to zero. Net force acting on the block is $\mathbf{f_T}^{k+1}(t + \Delta t) = m\mathbf{g}$, where $\mathbf{g}$ is the acceleration due to gravity, and net torque acting on the block is $\boldsymbol{\tau_T}^{k+1}(t + \Delta t) = \mathbf{0}$. Since the total force and total torque acting on the block are known now, we proceed to **Step 5** of the algorithm.

If, on the other hand, at least one point of the block is in contact with the ground, then we go through

Steps 3 and **4** to prevent the block from penetrating into the pedestal at this contact point. We start by attaching a coordinate system local to each contact point. The outward normal ($\boldsymbol{n_\alpha}$) to the pedestal at contact point α is known from the surface of the pedestal. The unit vectors $\boldsymbol{x_\alpha}$ and $\boldsymbol{y_\alpha}$ in the tangential directions to the pedestal surface are obtained by:

$$\boldsymbol{x_\alpha} = \frac{\hat{\mathbf{x}} - (\hat{\mathbf{x}} \cdot \boldsymbol{n_\alpha})\boldsymbol{n_\alpha}}{\|\hat{\mathbf{x}} - (\hat{\mathbf{x}} \cdot \boldsymbol{n_\alpha})\boldsymbol{n_\alpha}\|_2}; \qquad \boldsymbol{y_\alpha} = \frac{\boldsymbol{n_\alpha} \times \boldsymbol{x_\alpha}}{\|\boldsymbol{n_\alpha} \times \boldsymbol{x_\alpha}\|_2} \tag{12}$$

Here, $\hat{\mathbf{x}} = \{1, 0, 0\}$, the unit vector in the global X direction. For the above example of a rigid cuboid sitting on horizontal ground, $\boldsymbol{n_\alpha} = \{0, 0, 1\}$, $\boldsymbol{x_\alpha} = \{1, 0, 0\}$ and $\boldsymbol{y_\alpha} = \{0, 1, 0\}$ at all contact points.

Step 3: Resolve collisions by applying impulses.

The aim of this step is to ensure that the block is not moving towards the pedestal at any of the contact points. If contact point α of the block is moving towards the pedestal, then normal ($j_{n\alpha}\boldsymbol{n_\alpha}$) and frictional impulses ($j_{x\alpha}\boldsymbol{x_\alpha}$ and $j_{y\alpha}\boldsymbol{y_\alpha}$) are applied there in order to instantaneously change its velocity. Say there are q contact points. Let $\mathbf{j} = [\mathbf{j_n}\ \mathbf{j_x}\ \mathbf{j_y}]$, where $\mathbf{j_n} = [j_{n1}\ j_{n2}\ ...\ j_{nq}]$ etc., be the row vector of length $1 \times 3q$ containing the magnitudes of impulses applied at all contact points with respect to their local coordinate systems. Similarly, let $\dot{\mathbf{u}}^- = [\dot{\mathbf{u}}_\mathbf{n}^-\ \dot{\mathbf{u}}_\mathbf{x}^-\ \dot{\mathbf{u}}_\mathbf{y}^-]$ and $\dot{\mathbf{u}}^+ = [\dot{\mathbf{u}}_\mathbf{n}^+\ \dot{\mathbf{u}}_\mathbf{x}^+\ \dot{\mathbf{u}}_\mathbf{y}^+]$, where $\dot{\mathbf{u}}_\mathbf{n}^- = [\dot{u}_{n1}^-\ \dot{u}_{n2}^-\ ...\ \dot{u}_{nq}^-]$ etc., be the row vectors of length $1 \times 3q$ containing relative velocities of the contact points on the block with respect to the pedestal before and after collision, respectively.

Let $\dot{\mathbf{u}}_\mathbf{cm}^- = \dot{\mathbf{u}}_\mathbf{cm}^{k+1}(t+\Delta t)$ and $\boldsymbol{\omega}^- = \boldsymbol{\omega}^{k+1}(t+\Delta t)$ be the translational and angular velocity, respectively, of the block before collision. Let $\dot{\mathbf{u}}_\mathbf{cm}^+$ and $\boldsymbol{\omega}^+$ be the translational and angular velocity, respectively, of the block after collision with the pedestal. To simplify notation, let $\boldsymbol{r_\beta} = \boldsymbol{r_\beta}^{k+1}(t + \Delta t)$ be the position vector of contact point β with respect to the center of mass, and $\mathbf{I} = \mathbf{I}^{k+1}(t + \Delta t)$ be the moment of inertia of the block about cm in the global coordinate system. The translational and angular velocity of the block after collision may be obtained as follows:

$$\dot{\mathbf{u}}_\mathbf{cm}^+ = \frac{1}{m}\sum_{\beta=1}^{q} j_{n\beta}\boldsymbol{n_\beta} + \frac{1}{m}\sum_{\beta=1}^{q} j_{x\beta}\boldsymbol{x_\beta} + \frac{1}{m}\sum_{\beta=1}^{q} j_{y\beta}\boldsymbol{y_\beta} + \dot{\mathbf{u}}_\mathbf{cm}^- \tag{13}$$

$$\boldsymbol{\omega}^+ = \sum_{\beta=1}^{q} \mathbf{I}^{-1}(\boldsymbol{r_\beta} \times j_{n\beta}\boldsymbol{n_\beta}) + \sum_{\beta=1}^{q} \mathbf{I}^{-1}(\boldsymbol{r_\beta} \times j_{x\beta}\boldsymbol{x_\beta}) + \sum_{\beta=1}^{q} \mathbf{I}^{-1}(\boldsymbol{r_\beta} \times j_{y\beta}\boldsymbol{y_\beta}) + \boldsymbol{\omega}^- \tag{14}$$

The relative normal velocity of contact point α with respect to pedestal before and after collision are given by $\dot{u}_{n\alpha}^- = \boldsymbol{n_\alpha} \cdot [\dot{\mathbf{u}}_\mathbf{cm}^- + \boldsymbol{\omega}^- \times \boldsymbol{r_\alpha} - \dot{\mathbf{u}}_\mathbf{p}(t + \Delta t)]$ and $\dot{u}_{n\alpha}^+ = \boldsymbol{n_\alpha} \cdot [\dot{\mathbf{u}}_\mathbf{cm}^+ + \boldsymbol{\omega}^+ \times \boldsymbol{r_\alpha} - \dot{\mathbf{u}}_\mathbf{p}(t + \Delta t)]$, respectively. Similar expressions exist for the relative tangential velocities. Substituting for $\dot{\mathbf{u}}_\mathbf{cm}^+$ and $\boldsymbol{\omega}^+$ from Eqs. 13 and 14 into these expressions for relative velocities after collision, the affine relation between relative velocities after collision and the impulses may be obtained as follows:

$$\dot{\mathbf{u}}^+ = \mathbf{jC} + \mathbf{d}; \qquad \mathbf{C} = \begin{bmatrix} \mathbf{C_{nn}} & \mathbf{C_{nx}} & \mathbf{C_{ny}} \\ \mathbf{C_{xn}} & \mathbf{C_{xx}} & \mathbf{C_{xy}} \\ \mathbf{C_{yn}} & \mathbf{C_{yx}} & \mathbf{C_{yy}} \end{bmatrix}_{3q \times 3q}; \qquad \mathbf{d} = \begin{bmatrix} \mathbf{d_n} & \mathbf{d_x} & \mathbf{d_y} \end{bmatrix}_{1 \times 3q} \tag{15}$$

$$(C_{nn})_{\alpha\beta} = \frac{1}{m}\boldsymbol{n_\alpha} \cdot \boldsymbol{n_\beta} + (\boldsymbol{r_\alpha} \times \boldsymbol{n_\alpha})^T \mathbf{I}^{-1}(\boldsymbol{r_\beta} \times \boldsymbol{n_\beta}); \qquad \mathbf{d_n} = \dot{\mathbf{u}}_\mathbf{n}^-$$

$$(C_{xx})_{\alpha\beta} = \frac{1}{m}\boldsymbol{x_\alpha} \cdot \boldsymbol{x_\beta} + (\boldsymbol{r_\alpha} \times \boldsymbol{x_\alpha})^T \mathbf{I}^{-1}(\boldsymbol{r_\beta} \times \boldsymbol{x_\beta}); \qquad \mathbf{d_x} = \dot{\mathbf{u}}_\mathbf{x}^-$$

$$(C_{yy})_{\alpha\beta} = \frac{1}{m}\boldsymbol{y_\alpha} \cdot \boldsymbol{y_\beta} + (\boldsymbol{r_\alpha} \times \boldsymbol{y_\alpha})^T \mathbf{I}^{-1}(\boldsymbol{r_\beta} \times \boldsymbol{y_\beta}); \qquad \mathbf{d_y} = \dot{\mathbf{u}}_\mathbf{y}^-$$

$$(C_{nx})_{\alpha\beta} = (C_{xn})_{\beta\alpha} = \frac{1}{m}\boldsymbol{n_\alpha} \cdot \boldsymbol{x_\beta} + (\boldsymbol{r_\alpha} \times \boldsymbol{n_\alpha})^T \mathbf{I}^{-1}(\boldsymbol{r_\beta} \times \boldsymbol{x_\beta}); \qquad \alpha = 1, 2, ..., q$$

$$(C_{ny})_{\alpha\beta} = (C_{yn})_{\beta\alpha} = \frac{1}{m}\boldsymbol{n_\alpha} \cdot \boldsymbol{y_\beta} + (\boldsymbol{r_\alpha} \times \boldsymbol{n_\alpha})^T \mathbf{I}^{-1}(\boldsymbol{r_\beta} \times \boldsymbol{y_\beta}); \qquad \beta = 1, 2, ..., q$$

$$(C_{xy})_{\alpha\beta} = (C_{yx})_{\beta\alpha} = \frac{1}{m}\boldsymbol{x_\alpha} \cdot \boldsymbol{y_\beta} + (\boldsymbol{r_\alpha} \times \boldsymbol{x_\alpha})^T \mathbf{I}^{-1}(\boldsymbol{r_\beta} \times \boldsymbol{y_\beta});$$

There are a few constraints which the impulses ($\mathbf{j}$) and the relative velocities after collision ($\dot{\mathbf{u}}^+$) must satisfy. If a contact point α of the block is moving towards the pedestal (i.e., $\dot{u}^-_{n\alpha} < 0$), the normal impulse at α should push the point away from the pedestal to avoid interpenetration, i.e., $j_{n\alpha} \geq 0$. Next, from Newton's law of restitution, if e is the coefficient of restitution, then $\dot{u}^+_{n\alpha} = -e\dot{u}^-_{n\alpha}$. However, if the block is moving towards the pedestal at multiple contact points, the effect of the impulses applied at other points also affect the velocity at α as shown by Eq. 15. Therefore, Newton's law of restitution is the lower bound to the velocity after collision, i.e., $\dot{u}^+_{n\alpha} \geq -e\dot{u}^-_{n\alpha}$. Once $\dot{u}^+_{n\alpha}$ is above this lower bound, there is no longer a need for an impulse at that point, i.e., $j_{n\alpha} = 0$. This constraint can be expressed by the complementarity condition $j_{n\alpha}(\dot{u}^+_{n\alpha} + e\dot{u}^-_{n\alpha}) = 0$.

Because the impulses are applied instantaneously, no tangible displacement results. Therefore, static Coulomb friction laws are imposed on the friction impulses. This implies that the friction impulses should lie within/on the friction cone, i.e., $\sqrt{{j_{x\alpha}}^2 + {j_{y\alpha}}^2} \leq \mu_s j_{n\alpha}$, where μ_s is the static coefficient of friction. Also, the friction impulses should oppose the tangential velocity. In the earlier work by Baraff, this condition is implemented local to each contact point, i.e., the friction impulses at each contact point opposes the corresponding tangential velocity ($\dot{u}_{x\alpha} j_{x\alpha} + \dot{u}_{y\alpha} j_{y\alpha} \leq 0$). However, as seen from Eq. 15, the tangential velocity at contact point α is influenced by the friction impulses at all contact points. Therefore, the friction impulses must collectively oppose the tangential velocity at all contact points and result in the least magnitude of tangential velocity at all contact points.

The problem described above can be solved in many ways. Baraff [2] tackles it sequentially one contact point at a time. As illustrated earlier, this leads to different solutions based on the ordering of the contact points. We resolve this problem by collectively solving for all contact points first the normal impulse forces, and then the friction impulse forces. Because these forces are coupled, we repeat this exercise several times in an iterative fashion until there is little change in the forces (to within a tolerance). The computations in impulse iteration $p+1$ within time step iteration $k+1$ are described next. To start the iteration, all impulses are initialized to zero.

Step 3(a): Calculating normal impulses.

Using the normal part of Eq. 15 and the vectorized form of normal impulse constraints, the normal impulse problem is recast as a minimization problem:

$$\left.\begin{aligned} &\dot{\mathbf{u}}_\mathbf{n}^+ = {\mathbf{j}_\mathbf{n}}^{p+1}\mathbf{C_{nn}} + {\mathbf{j}_\mathbf{x}}^{p}\mathbf{C_{xn}} + {\mathbf{j}_\mathbf{y}}^{p}\mathbf{C_{yn}} + \mathbf{d_n} \\ &{\mathbf{j}_\mathbf{n}}^{p+1} \geq \mathbf{0}; \quad \dot{\mathbf{u}}_\mathbf{n}^+ + e\dot{\mathbf{u}}_\mathbf{n}^- \geq \mathbf{0} \\ &{\mathbf{j}_\mathbf{n}}^{p+1}(\dot{\mathbf{u}}_\mathbf{n}^+ + e\dot{\mathbf{u}}_\mathbf{n}^-)^T = 0 \end{aligned}\right\} \implies \begin{aligned} \text{minimize} \quad & {\mathbf{j}_\mathbf{n}}^{p+1}({\mathbf{j}_\mathbf{n}}^{p+1}\mathbf{C_{nn}} + {\mathbf{d}_\mathbf{n}}')^T \\ \text{subject to} \quad & {\mathbf{j}_\mathbf{n}}^{p+1} \geq \mathbf{0} \\ & {\mathbf{j}_\mathbf{n}}^{p+1}\mathbf{C_{nn}} + {\mathbf{d}_\mathbf{n}}' \geq \mathbf{0} \end{aligned} \tag{16}$$

Here, ${\mathbf{d}_\mathbf{n}}' = {\mathbf{j}_\mathbf{x}}^{p}\mathbf{C_{xn}} + {\mathbf{j}_\mathbf{y}}^{p}\mathbf{C_{yn}} + (1+e)\mathbf{d_n}$. This quadratic programming (QP) problem with an objective function having an optimal value of zero is known as a Linear Complementarity Problem (LCP). Baraff [2] has shown that the matrix $\mathbf{C}$ is positive semi-definite. This implies that sub-matrix $\mathbf{C_{nn}}$ is also positive semi-definite. This LCP is feasible, i.e., there exists a ${\mathbf{j}_\mathbf{n}}^{p+1}$ satisfying all the inequality constraints in Eq. 16 (details in appendix). It is also known that this LCP is solvable for every ${\mathbf{d}_\mathbf{n}}'$ if $\mathbf{C_{nn}}$ is positive semi-definite and the problem is feasible [9]. However, the positive semi-definiteness of the matrix also implies that the LCP/QP may have infinitely many solutions.

Here, we solve this LCP using the Sequential Quadratic Programming (SQP) algorithm [19] of the open source nonlinear optimization software NLopt [14]. Starting from ${\mathbf{j}_\mathbf{n}}^{p}$ the optimal solution for ${\mathbf{j}_\mathbf{n}}^{p+1}$ is calculated iteratively based on the local gradient of the objective function (similar to a Newton-Raphson iteration). The resulting solution, therefore, is the solution that is closest to ${\mathbf{j}_\mathbf{n}}^{p}$ from the infinite set of solutions, i.e., $\|{\mathbf{j}_\mathbf{n}}^{p+1} - {\mathbf{j}_\mathbf{n}}^{p}\|_2$ is the minimum among all possible solutions to the LCP.

Step 3(b): Calculating friction impulses.

The friction part of Eq. 15 is:

$$\begin{bmatrix} \dot{\mathbf{u}}_\mathbf{x}^+ & \dot{\mathbf{u}}_\mathbf{y}^+ \end{bmatrix} = \begin{bmatrix} \mathbf{j_x} & \mathbf{j_y} \end{bmatrix}^{r+1} \begin{bmatrix} \mathbf{C_{xx}} & \mathbf{C_{xy}} \\ \mathbf{C_{yx}} & \mathbf{C_{yy}} \end{bmatrix} + \mathbf{j_n}^{p+1} \begin{bmatrix} \mathbf{C_{nx}} & \mathbf{C_{ny}} \end{bmatrix} + \begin{bmatrix} \mathbf{d_x} & \mathbf{d_y} \end{bmatrix} \tag{17}$$

This equation along with the friction impulse constraints constitute the friction impulse problem. As mentioned previously, there are two constraints on the friction impulses: first, they should lie on/inside the friction cone, and second, they should collectively oppose the tangential velocity at all contact points. These constraints are considered one by one and the problem is solved iteratively. The computations involved in friction impulse iteration $r+1$ within impulse iteration $p+1$ are described next.

First, we define two sets to classify contact points in each friction impulse iteration: $\mathbf{S}^r$ and $\bar{\mathbf{S}}^r$. $\bar{\mathbf{S}}^r$ contains contact points that lie on the surface of the friction cone whose friction forces are assumed to remain unchanged as long as the point belongs to this set. Set $\mathbf{S}^r$ contains the remaining contact points. Let set $\mathbf{N} = \{1, 2, ..., q\}$ represent the set of all contact points. At the start of the friction impulse iteration, set $\mathbf{S}^0$ contains all the contact points and set $\bar{\mathbf{S}}^0$ is empty, i.e., $\mathbf{S}^0 = \mathbf{N}$ and $\bar{\mathbf{S}}^0 = \varnothing$.

Step 3(b)(i): Satisfying the "friction impulses oppose tangential velocity" constraint.

In this step, the friction impulses (${j_{x\alpha}}^{r+1}$ and ${j_{y\alpha}}^{r+1}$) for all contact points $\alpha \in \mathbf{S}^r$ are calculated such that the relative tangential velocities of contact points in this set are reduced to zero. As per the definition of set $\bar{\mathbf{S}}^r$, the friction impulses of all contact points $\alpha \in \bar{\mathbf{S}}^r$ are left unchanged, i.e., ${j_{x\alpha}}^{r+1} = {j_{x\alpha}}^r$ and ${j_{y\alpha}}^{r+1} = {j_{y\alpha}}^r$. For ease of notation, let $\mathbf{j_{x,S}}^{r+1}$ be the vector of frictional impulses in x direction for all contact points in $\mathbf{S}^r$, and $\mathbf{C_{xx,SS}}$ be the sub-matrix of $\mathbf{C_{xx}}$ corresponding to the contact points in $\mathbf{S}^r$, and so on. Also let, $\mathbf{j_{x,S}}^{r+1} = \mathbf{j_{x,S}}^r + \Delta\mathbf{j_{x,S}}$ and $\mathbf{j_{y,S}}^{r+1} = \mathbf{j_{y,S}}^r + \Delta\mathbf{j_{y,S}}$. Using this relation, re-arranging the terms in Eq. 17 and setting the tangential velocities for all contact points in set $\mathbf{S}^r$ equal to zero gives:

$$\begin{aligned} \begin{bmatrix} \mathbf{0} & \mathbf{0} \end{bmatrix} &= \begin{bmatrix} \mathbf{j_{x,S}} & \mathbf{j_{y,S}} \end{bmatrix}^{r+1} \underbrace{\begin{bmatrix} \mathbf{C_{xx,SS}} & \mathbf{C_{xy,SS}} \\ \mathbf{C_{yx,SS}} & \mathbf{C_{yy,SS}} \end{bmatrix}}_{\mathbf{C'}} \\ &+ \underbrace{\begin{bmatrix} \mathbf{j_{x,\bar{S}}} & \mathbf{j_{y,\bar{S}}} \end{bmatrix}^{r+1} \begin{bmatrix} \mathbf{C_{xx,\bar{S}S}} & \mathbf{C_{xy,\bar{S}S}} \\ \mathbf{C_{yx,\bar{S}S}} & \mathbf{C_{yy,\bar{S}S}} \end{bmatrix} + \mathbf{j_n}^{p+1} \begin{bmatrix} \mathbf{C_{nx,NS}} & \mathbf{C_{ny,NS}} \end{bmatrix} + \begin{bmatrix} \mathbf{d_{x,S}} & \mathbf{d_{y,S}} \end{bmatrix}}_{\mathbf{d'}} \\ \implies \begin{bmatrix} \Delta\mathbf{j_{x,S}} & \Delta\mathbf{j_{y,S}} \end{bmatrix} &= -\mathbf{d'}(\mathbf{C'})^{-1} - \begin{bmatrix} \mathbf{j_{x,S}} & \mathbf{j_{y,S}} \end{bmatrix}^r \mathbf{C'}(\mathbf{C'})^{-1} \end{aligned} \tag{18}$$

The matrix $\mathbf{C'}$ may in general be rank deficient. So, there may exist infinitely many solutions for $[\Delta\mathbf{j_{x,S}}\ \Delta\mathbf{j_{y,S}}]$ from the above set of linear equations. However, if the Moore-Penrose pseudo inverse is used for ${\mathbf{C'}}^{-1}$, then the resulting solution for $[\Delta\mathbf{j_{x,S}}\ \Delta\mathbf{j_{y,S}}]$ is the solution with the least 2-norm. This implies that $[\mathbf{j_x}\ \mathbf{j_y}]^{r+1}$ is the solution closest to $[\mathbf{j_x}\ \mathbf{j_y}]^r$.

Step 3(b)(ii): Satisfying the friction cone constraint.

If friction impulses calculated in the previous step lie outside the friction cone for any point α in $\mathbf{S}^r$, a scaling factor σ_α is applied to $\Delta j_{x\alpha}$ and $\Delta j_{y\alpha}$ in order to project the friction impulses back to the surface of the friction cone as shown below:

$$(j_{x\alpha}^r + \sigma_\alpha \Delta j_{x\alpha})^2 + (j_{y\alpha}^r + \sigma_\alpha \Delta j_{y\alpha})^2 = \mu_s^2 (j_{n\alpha}^{p+1})^2 \tag{19}$$

The positive root of the above quadratic expression is used for σ_α. The contact point $\alpha \in \mathbf{S}^r$ which has the maximum scaling factor (say $\bar{\alpha}$) is then moved to set $\bar{\mathbf{S}}^{r+1}$. This implies that $\mathbf{S}^{r+1} = \mathbf{S}^r \setminus \{\bar{\alpha}\}$ and $\bar{\mathbf{S}}^{r+1} = \bar{\mathbf{S}}^r \cup \{\bar{\alpha}\}$. In accordance with the definition of set $\bar{\mathbf{S}}^{r+1}$, the friction impulses for $\bar{\alpha}$ lie on the surface of the friction cone, and do not change in magnitude or direction as long as it remains in this set. The relative tangential velocity ($\dot{u}_{x\bar{\alpha}}^+$ and $\dot{u}_{y\bar{\alpha}}^+$) when the contact point $\bar{\alpha}$ enters $\bar{\mathbf{S}}^{r+1}$ is stored into $\dot{u}_{x\bar{\alpha}}$ and $\dot{u}_{y\bar{\alpha}}$. In a future friction impulse iteration, if $\dot{u}_{x\bar{\alpha}}^+$ or $\dot{u}_{y\bar{\alpha}}^+$ differ in sign from $\dot{u}_{x\bar{\alpha}}$ or $\dot{u}_{y\bar{\alpha}}$, respectively, then $\bar{\alpha}$ is released from $\bar{\mathbf{S}}$ back to $\mathbf{S}$. This method of dividing the contact points into sets $\mathbf{S}^{r+1}$ and $\bar{\mathbf{S}}^{r+1}$ offers

a simple termination condition for the friction impulse iteration, ensuring convergence is achieved within a few iterations.

Step 3(b)(iii): Termination condition for the friction impulse iteration.

At the end of **Step 3(b)(ii)**, three things can happen: a point may move from $\mathbf{S}^r$ to $\bar{\mathbf{S}}^{r+1}$, few points may move from $\bar{\mathbf{S}}^{r+1}$ to $\mathbf{S}^{r+1}$, or the sets $\mathbf{S}^{r+1}$ and $\bar{\mathbf{S}}^{r+1}$ remain unchanged from previous friction impulse iteration, i.e., $\mathbf{S}^{r+1} = \mathbf{S}^r$ and $\bar{\mathbf{S}}^{r+1} = \bar{\mathbf{S}}^r$. In the first two scenarios, the algorithm goes back to **Step 3(b)(i)** and continues to the next friction impulse iteration. In the third scenario, when the sets remain unchanged, the friction impulse iteration is terminated with $\mathbf{j_x}^{p+1} = \mathbf{j_x}^{r+1}$ and $\mathbf{j_y}^{p+1} = \mathbf{j_y}^{r+1}$.

Step 3(c): Termination condition for the impulse iteration.

After convergence of the friction impulses $\mathbf{j_x}^{p+1}$ and $\mathbf{j_y}^{p+1}$, the algorithm goes back to **Step 3(a)** for the next impulse iteration. The impulse iteration is terminated when the relative change in the normal impulses from the previous impulse iteration is less than a tolerance ϵ_1, i.e., $\|\mathbf{j_n}^{p+1} - \mathbf{j_n}^{p}\|_2 \leq \epsilon_1 \|\mathbf{j_n}^{p}\|_2$. After termination, $\dot{\mathbf{u}}^+_{\mathbf{cm}}$ and $\boldsymbol{\omega}^+$ are calculated using Eqs. 13 and 14, and $\dot{\mathbf{u}}^{k+1}_{\mathbf{cm}}(t+\Delta t)$ and $\mathbf{l}^{k+1}(t+\Delta t)$ are updated as follows:

$$\dot{\mathbf{u}}^{k+1}_{\mathbf{cm}}(t+\Delta t) = \dot{\mathbf{u}}^+_{\mathbf{cm}} \tag{20}$$

$$\mathbf{l}^{k+1}(t+\Delta t) = \mathbf{l}^{k+1}(t+\Delta t) + \sum_{\beta=1}^{q} \boldsymbol{r_\beta} \times j_{n\beta}\boldsymbol{n_\beta} + \sum_{\beta=1}^{q} \boldsymbol{r_\beta} \times j_{x\beta}\boldsymbol{x_\beta} + \sum_{\beta=1}^{q} \boldsymbol{r_\beta} \times j_{y\beta}\boldsymbol{y_\beta} \tag{21}$$

Step 4: Computing the contact forces.

The aim of this step is to calculate contact forces to prevent the block from accelerating towards the pedestal at the contact points. Let $\mathbf{f} = [\mathbf{f_n}\ \mathbf{f_x}\ \mathbf{f_y}]$, where $\mathbf{f_n} = [f_{n1}\ f_{n2}\ ...\ f_{nq}]$ etc., be the row vector of length $1 \times 3q$ containing the magnitudes of forces applied at all contact points with respect to their local coordinate systems. Similarly, let $\ddot{\mathbf{u}} = [\ddot{\mathbf{u}}_\mathbf{n}\ \ddot{\mathbf{u}}_\mathbf{x}\ \ddot{\mathbf{u}}_\mathbf{y}]$ be the relative acceleration of the contact points on the block with respect to the pedestal. The translational ($\ddot{\mathbf{u}}_\mathbf{cm}$) and rotational ($\dot{\boldsymbol{\omega}}$) acceleration of the block are given by:

$$\ddot{\mathbf{u}}_\mathbf{cm} = \frac{1}{m}\sum_{\beta=1}^{q} f_{n\beta}\boldsymbol{n_\beta} + \frac{1}{m}\sum_{\beta=1}^{q} f_{x\beta}\boldsymbol{x_\beta} + \frac{1}{m}\sum_{\beta=1}^{q} f_{y\beta}\boldsymbol{y_\beta} + \mathbf{g} \tag{22}$$

$$\dot{\boldsymbol{\omega}} = \sum_{\beta=1}^{q} \mathbf{I}^{-1}(\boldsymbol{r_\beta} \times f_{n\beta}\boldsymbol{n_\beta}) + \sum_{\beta=1}^{q} \mathbf{I}^{-1}(\boldsymbol{r_\beta} \times f_{x\beta}\boldsymbol{x_\beta}) + \sum_{\beta=1}^{q} \mathbf{I}^{-1}(\boldsymbol{r_\beta} \times f_{y\beta}\boldsymbol{y_\beta}) + \mathbf{I}^{-1}(\mathbf{l} \times \boldsymbol{w}) \tag{23}$$

Here, $\mathbf{I}^{-1} = [\mathbf{I}^{k+1}(t+\Delta t)]^{-1}$, $\mathbf{l} = \mathbf{l}^{k+1}(t+\Delta t)$, $\boldsymbol{r_\beta} = \boldsymbol{r_\beta}^{k+1}(t+\Delta t)$, $\boldsymbol{\omega} = \mathbf{I}^{-1}\mathbf{l}$, $\ddot{\mathbf{u}}_\mathbf{p} = \ddot{\mathbf{u}}_\mathbf{p}(t+\Delta t)$, and $\mathbf{g}$ is the acceleration due to gravity in the global coordinate system.

Now, the normal acceleration of contact point α relative to the pedestal is given by $\ddot{u}_{n\alpha} = \boldsymbol{n_\alpha} \cdot [\ddot{\mathbf{u}}_\mathbf{cm} + \dot{\boldsymbol{\omega}} \times \boldsymbol{r_\alpha} + \boldsymbol{\omega} \times (\boldsymbol{\omega} \times \boldsymbol{r_\alpha}) - \ddot{\mathbf{u}}_\mathbf{p}]$. Similar relations exist for the relative tangential accelerations ($\ddot{u}_{x\alpha}$ and $\ddot{u}_{y\alpha}$) of contact point α. Substituting for $\ddot{\mathbf{u}}_\mathbf{cm}$ and $\dot{\boldsymbol{\omega}}$ from Eqs. 22 and 23 into the above expressions, the affine

relation between the relative accelerations and contact forces at all contact points is obtained:

$$\ddot{\mathbf{u}} = \mathbf{fA} + \mathbf{b}; \qquad \mathbf{A} = \underset{3q\times 3q}{\begin{bmatrix} \mathbf{A_{nn}} & \mathbf{A_{nx}} & \mathbf{A_{ny}} \\ \mathbf{A_{xn}} & \mathbf{A_{xx}} & \mathbf{A_{xy}} \\ \mathbf{A_{yn}} & \mathbf{A_{yx}} & \mathbf{A_{yy}} \end{bmatrix}}; \qquad \mathbf{b} = \underset{1\times 3q}{\begin{bmatrix} \mathbf{b_n} & \mathbf{b_x} & \mathbf{b_y} \end{bmatrix}} \tag{24}$$

$$(A_{nn})_{\alpha\beta} = \frac{1}{m}\boldsymbol{n_\alpha}\cdot\boldsymbol{n_\beta} + (\boldsymbol{r_\alpha}\times\boldsymbol{n_\alpha})^T\mathbf{I}^{-1}(\boldsymbol{r_\beta}\times\boldsymbol{n_\beta});$$

$$(A_{xx})_{\alpha\beta} = \frac{1}{m}\boldsymbol{x_\alpha}\cdot\boldsymbol{x_\beta} + (\boldsymbol{r_\alpha}\times\boldsymbol{x_\alpha})^T\mathbf{I}^{-1}(\boldsymbol{r_\beta}\times\boldsymbol{x_\beta});$$

$$(A_{yy})_{\alpha\beta} = \frac{1}{m}\boldsymbol{y_\alpha}\cdot\boldsymbol{y_\beta} + (\boldsymbol{r_\alpha}\times\boldsymbol{y_\alpha})^T\mathbf{I}^{-1}(\boldsymbol{r_\beta}\times\boldsymbol{y_\beta});$$

$$(A_{xn})_{\beta\alpha} = (A_{nx})_{\alpha\beta} = \frac{1}{m}\boldsymbol{n_\alpha}\cdot\boldsymbol{x_\beta} + (\boldsymbol{r_\alpha}\times\boldsymbol{n_\alpha})^T\mathbf{I}^{-1}(\boldsymbol{r_\beta}\times\boldsymbol{x_\beta});$$

$$(A_{yn})_{\beta\alpha} = (A_{ny})_{\alpha\beta} = \frac{1}{m}\boldsymbol{n_\alpha}\cdot\boldsymbol{y_\beta} + (\boldsymbol{r_\alpha}\times\boldsymbol{n_\alpha})^T\mathbf{I}^{-1}(\boldsymbol{r_\beta}\times\boldsymbol{y_\beta});$$

$$(A_{yx})_{\beta\alpha} = (A_{xy})_{\alpha\beta} = \frac{1}{m}\boldsymbol{x_\alpha}\cdot\boldsymbol{y_\beta} + (\boldsymbol{r_\alpha}\times\boldsymbol{x_\alpha})^T\mathbf{I}^{-1}(\boldsymbol{r_\beta}\times\boldsymbol{y_\beta});$$

$$b_{n\alpha} = \boldsymbol{n_\alpha}\cdot[\mathbf{g} + \mathbf{I}^{-1}(\mathbf{l}\times\boldsymbol{w})\times\boldsymbol{r_\alpha} + \boldsymbol{\omega}\times(\boldsymbol{\omega}\times\boldsymbol{r_\alpha}) - \ddot{\mathbf{u}}_\mathbf{p}]$$

$$b_{x\alpha} = \boldsymbol{x_\alpha}\cdot[\mathbf{g} + \mathbf{I}^{-1}(\mathbf{l}\times\boldsymbol{w})\times\boldsymbol{r_\alpha} + \boldsymbol{\omega}\times(\boldsymbol{\omega}\times\boldsymbol{r_\alpha}) - \ddot{\mathbf{u}}_\mathbf{p}]$$

$$b_{y\alpha} = \boldsymbol{y_\alpha}\cdot[\mathbf{g} + \mathbf{I}^{-1}(\mathbf{l}\times\boldsymbol{w})\times\boldsymbol{r_\alpha} + \boldsymbol{\omega}\times(\boldsymbol{\omega}\times\boldsymbol{r_\alpha}) - \ddot{\mathbf{u}}_\mathbf{p}]$$

The contact points are divided into two sets $\mathbf{R}$ and $\mathbf{D}$ based on the relative tangential velocity. If the relative tangential velocity of a contact point is zero (within a tolerance), then the point belongs to set $\mathbf{R}$, or else the contact point belongs to set $\mathbf{D}$. There are a few constraints on the contact forces ($\mathbf{f}$) and the relative accelerations ($\ddot{\mathbf{u}}$): (i) The normal force at any contact point α should be non-negative, i.e., ($f_{n\alpha} \geq 0$). This condition ensures that the forces only push the block and the pedestal away and do not make them stick together. (ii) The block and pedestal should not accelerate towards each other at the contact points, i.e., $\ddot{u}_{n\alpha} \geq 0$. (iii) Normal forces are applied only to make the relative normal accelerations at contact points non-negative, these forces should be zero if this condition is already satisfied at a contact point (i.e., $f_{n\alpha}\ddot{u}_{n\alpha} = 0$).

The conditions on the friction forces vary depending on whether a contact point belongs to set $\mathbf{R}$ or $\mathbf{D}$. For a contact point α with zero relative tangential velocity and belonging to $\mathbf{R}$, the forces of friction must satisfy the laws of static Coulomb friction, i.e., the friction forces should lie on/within the friction cone $\sqrt{{f_{x\alpha}}^2 + {f_{y\alpha}}^2} \leq \mu_s(f_{n\alpha})$, and they should oppose the tangential acceleration. As in the case of the impulses, the friction forces should collectively oppose the tangential acceleration of all contact points belonging to $\mathbf{R}$ resulting in the least magnitude of tangential acceleration at these contact points. For a contact point α with non-zero relative tangential velocity and belonging to $\mathbf{D}$, the forces of friction must comply with laws of kinetic Coulomb friction, i.e., the magnitude of the friction force is $\mu_d f_{n\alpha}$ and the friction forces should directly oppose the relative tangential velocity. Thus,

$$f_{x\alpha} = -\frac{\dot{u}_{x\alpha}}{\sqrt{\dot{u}_{x\alpha}^2 + \dot{u}_{y\alpha}^2}}\mu_d f_{n\alpha}; \quad f_{y\alpha} = -\frac{\dot{u}_{y\alpha}}{\sqrt{\dot{u}_{x\alpha}^2 + \dot{u}_{y\alpha}^2}}\mu_d f_{n\alpha} \quad \forall\alpha \in \mathbf{D} \tag{25}$$

Here, μ_d is the kinetic coefficient of friction between the block and the pedestal. Contact forces are computed iteratively (iterations denoted by "p") in two alternating steps in a manner analogous to impulse forces (**Step 3**), the first involving the computation of normal forces and the second involving the computation of frictional forces. The contact force iteration is initialized with the contact forces at time t. If the block is initially resting on the pedestal, the initial values of the contact forces are computed by imposing acceleration due to gravity alone on the block. The two-step contact force computation is described next.

Step 4(a): Computing normal contact forces.

For ease of notation, let $\mathbf{f_{n,R}}$ and $\mathbf{f_{n,D}}$ contain the vector of normal forces for all contact points belonging to sets $\mathbf{R}$ and $\mathbf{D}$, respectively. Similarly, let $\mathbf{A_{nn,RR}}$ be the sub-matrix of $\mathbf{A_{nn}}$ corresponding to the points in $\mathbf{R}$, and so on. Substituting Eq. 25 into the normal part of Eq. 24 and re-arranging, we get the following affine relation:

$$\begin{aligned}
\begin{bmatrix} \ddot{\mathbf{u}}_{\mathbf{n,R}} & \ddot{\mathbf{u}}_{\mathbf{n,D}} \end{bmatrix} &= \begin{bmatrix} \mathbf{f_{n,R}} & \mathbf{f_{n,D}} \end{bmatrix}^{p+1} \begin{bmatrix} \mathbf{A_{nn,RR}} & \mathbf{A_{nn,RD}} \\ \mathbf{A_{nn,DR}} & \mathbf{A_{nn,DD}} \end{bmatrix} \\
&\quad + \begin{bmatrix} \mathbf{f_{x,D}} & \mathbf{f_{y,D}} \end{bmatrix}^{p+1} \begin{bmatrix} \mathbf{A_{xn,DR}} & \mathbf{A_{xn,DD}} \\ \mathbf{A_{yn,DR}} & \mathbf{A_{yn,DD}} \end{bmatrix} \\
&\quad \underbrace{+ \begin{bmatrix} \mathbf{f_{x,R}} & \mathbf{f_{y,R}} \end{bmatrix}^{p+1} \begin{bmatrix} \mathbf{A_{xn,RR}} & \mathbf{A_{xn,RD}} \\ \mathbf{A_{yn,RR}} & \mathbf{A_{yn,RD}} \end{bmatrix} + \begin{bmatrix} \mathbf{b_{n,R}} & \mathbf{b_{n,D}} \end{bmatrix}^{p+1}}_{\mathbf{b'}} \\
\implies \begin{bmatrix} \ddot{\mathbf{u}}_{\mathbf{n,R}} & \ddot{\mathbf{u}}_{\mathbf{n,D}} \end{bmatrix} &= \begin{bmatrix} \mathbf{f_{n,R}} & \mathbf{f_{n,D}} \end{bmatrix}^{p+1} \underbrace{\begin{bmatrix} \mathbf{A_{nn,RR}} & \mathbf{A_{nn,RD}} \\ \mathbf{A'_{nn,DR}} & \mathbf{A'_{nn,DD}} \end{bmatrix}}_{\mathbf{A'}} + \mathbf{b'} \implies \ddot{\mathbf{u}}_{\mathbf{n}} = {\mathbf{f_n}}^{p+1}\mathbf{A'} + \mathbf{b'}
\end{aligned} \tag{26}$$

Here, $(A'_{nn})_{\alpha\beta} = (A_{nn})_{\alpha\beta} - \frac{\dot{u}_{x\alpha}}{\sqrt{\dot{u}_{x\alpha}^2+\dot{u}_{y\alpha}^2}}\mu_d(A_{xn})_{\alpha\beta} - \frac{\dot{u}_{y\alpha}}{\sqrt{\dot{u}_{x\alpha}^2+\dot{u}_{y\alpha}^2}}\mu_d(A_{yn})_{\alpha\beta}$ for $\alpha \in \mathbf{D}$ and $\beta \in \mathbf{R} \cup \mathbf{D}$. The affine relation between the $\ddot{\mathbf{u}}_\mathbf{n}$ and ${\mathbf{f_n}}^{p+1}$ from Eq. 26 along with the normal force constraints may be posed as the following QP:

$$\left.\begin{array}{c} \ddot{\mathbf{u}}_{\mathbf{n}} = {\mathbf{f_n}}^{p+1}\mathbf{A'} + \mathbf{b'} \\ {\mathbf{f_n}}^{p+1} \geq \mathbf{0}; \quad \ddot{\mathbf{u}}_{\mathbf{n}} \geq \mathbf{0} \\ {\mathbf{f_n}}^{p+1}\ddot{\mathbf{u}}_{\mathbf{n}}^T = 0 \end{array}\right\} \implies \begin{array}{ll} \text{minimize} & {\mathbf{f_n}}^{p+1}({\mathbf{f_n}}^{p+1}\mathbf{A'} + \mathbf{b'})^T \\ \text{subject to} & {\mathbf{f_n}}^{p+1} \geq \mathbf{0} \\ & {\mathbf{f_n}}^{p+1}\mathbf{A'} + \mathbf{b'} \geq \mathbf{0} \end{array} \tag{27}$$

As in the case of the impulses, this is an LCP, i.e., a special QP with the optimal value of objective function equal to zero. However, matrix $\mathbf{A'}$ is not necessarily symmetric or positive semi-definite. This poses a problem as existence of solution is mathematically guaranteed only when the matrix $\mathbf{A'}$ is positive definite or semi-definite or belongs to one of the special classes of matrices discussed in Chapter 3 of [9]. Fortunately, for realistic values of μ_d, the diagonal elements of $\mathbf{A'}$ are in general non-negative and solution does exist for the corresponding LCP. The solution, if and when it exists, may be estimated using an approach analogous to **Step 3(a)**.

Step 4(b): Computing contact frictional forces.

From the previous step, ${\mathbf{f_{n,D}}}^{p+1}$ is known, therefore, from Eq. 25, ${\mathbf{f_{x,D}}}^{p+1}$ and ${\mathbf{f_{y,D}}}^{p+1}$ are also known. The aim of this step is to calculate ${\mathbf{f_{x,R}}}^{p+1}$ and ${\mathbf{f_{y,R}}}^{p+1}$ such that they oppose $\ddot{\mathbf{u}}_{\mathbf{x,R}}$ and $\ddot{\mathbf{u}}_{\mathbf{y,R}}$, respectively, at all contact points within/on the static friction cone and belonging to $\mathbf{R}$. The friction part of the affine relation from Eq. 24 is re-ordered to get:

$$\begin{aligned}
\begin{bmatrix} \ddot{\mathbf{u}}_{\mathbf{x,R}} & \ddot{\mathbf{u}}_{\mathbf{y,R}} \end{bmatrix} &= \begin{bmatrix} \mathbf{f_{x,R}} & \mathbf{f_{y,R}} \end{bmatrix}^{p+1} \begin{bmatrix} \mathbf{A_{xx,RR}} & \mathbf{A_{xy,RR}} \\ \mathbf{A_{yx,RR}} & \mathbf{A_{yy,RR}} \end{bmatrix} \\
&\underbrace{+ \begin{bmatrix} \mathbf{f_{n,R}} & \mathbf{f_{n,D}} \end{bmatrix}^{p+1} \begin{bmatrix} \mathbf{A_{nx,RR}} & \mathbf{A_{ny,RR}} \\ \mathbf{A_{nx,DR}} & \mathbf{A_{ny,DR}} \end{bmatrix} + \begin{bmatrix} \mathbf{f_{x,D}} & \mathbf{f_{y,D}} \end{bmatrix}^{p+1} \begin{bmatrix} \mathbf{A_{xx,DR}} & \mathbf{A_{xy,DR}} \\ \mathbf{A_{yx,DR}} & \mathbf{A_{yy,DR}} \end{bmatrix} + \begin{bmatrix} \mathbf{b_{x,R}} & \mathbf{b_{y,R}} \end{bmatrix}}_{\begin{bmatrix} \mathbf{b'_{x,R}} & \mathbf{b'_{y,R}} \end{bmatrix}} \\
\implies \begin{bmatrix} \ddot{\mathbf{u}}_{\mathbf{x,R}} & \ddot{\mathbf{u}}_{\mathbf{y,R}} \end{bmatrix} &= \begin{bmatrix} \mathbf{f_{x,R}} & \mathbf{f_{y,R}} \end{bmatrix}^{p+1} \begin{bmatrix} \mathbf{A_{xx,RR}} & \mathbf{A_{xy,RR}} \\ \mathbf{A_{yx,RR}} & \mathbf{A_{yy,RR}} \end{bmatrix} + \begin{bmatrix} \mathbf{b'_{x,R}} & \mathbf{b'_{y,R}} \end{bmatrix}
\end{aligned} \tag{28}$$

This system is similar to Eq. 17 and is solved in a manner similar to **Step 3(b)**.

Step 4(c): Termination condition for the contact force iteration.

After computing the friction forces ${\mathbf{f_x}_{,\mathbf{R}}}^{p+1}$ and ${\mathbf{f_y}_{,\mathbf{R}}}^{p+1}$, the algorithm goes back to **Step 4(a)** for the next contact force iteration. This iteration is terminated when the relative change in the normal forces from the previous contact force iteration is less than a desired tolerance ϵ_1, i.e., $\|{\mathbf{f_n}}^{p+1} - {\mathbf{f_n}}^{p}\|_2 \leq \epsilon_1 \|{\mathbf{f_n}}^{p}\|_2$. Then, the total force ${\mathbf{f_T}}^{k+1}(t+\Delta t)$ and total torque ${\boldsymbol{\tau_T}}^{k+1}(t+\Delta t)$ acting on the block are given by:

$$ {\mathbf{f_T}}^{k+1}(t+\Delta t) = m\mathbf{g} + \sum_{\beta=1}^{q} f_{n\beta}\boldsymbol{n_\beta} + \sum_{\beta=1}^{q} f_{x\beta}\boldsymbol{x_\beta} + \sum_{\beta=1}^{q} f_{y\beta}\boldsymbol{y_\beta} \tag{29} $$

$$ {\boldsymbol{\tau_T}}^{k+1}(t+\Delta t) = \sum_{\beta=1}^{q} \boldsymbol{r_\beta} \times f_{n\beta}\boldsymbol{n_\beta} + \sum_{\beta=1}^{q} \boldsymbol{r_\beta} \times f_{x\beta}\boldsymbol{x_\beta} + \sum_{\beta=1}^{q} \boldsymbol{r_\beta} \times f_{y\beta}\boldsymbol{y_\beta} \tag{30} $$

Step 5: Termination condition for the time-step iteration k.

After obtaining the total force and torque acting on the block, the algorithm goes back to **Step 1** for the next time-step iteration. This iteration is terminated when the relative change in the total force and torque from the previous time-step iteration is less than the desired tolerance level ϵ_1, i.e., $\|{\mathbf{f_T}}^{k+1} - {\mathbf{f_T}}^{k}\|_2 \leq \epsilon_1 \|{\mathbf{f_T}}^{k}\|_2$ and $\|{\boldsymbol{\tau_T}}^{k+1} - {\boldsymbol{\tau_T}}^{k}\|_2 \leq \epsilon_1 \|{\boldsymbol{\tau_T}}^{k}\|_2$, and the state variables of the block are deemed to have converged at $t+\Delta t$. After convergence, the algorithm proceeds to the next time integration step. The convergence of the algorithm for each time-step iteration k is not guaranteed. If the number of time-step iterations k exceeds a user defined number of iterations (say 100), the time-step is reduced and the calculations are re-started for the reduced time step.

While it would be ideal for the algorithm to determine the contact force/impulse state that is closest to the previous state of the system (i.e., at time t), our algorithm determines the contact force/impulse state that is closest to the previous iteration of the current step (or the last iteration of the previous step if this is the first iteration of the current step) to achieve faster and more reliable convergence. For the types of problems considered in this paper, we have verified that the contact force/impulse configuration closest to the previous state of the system is same as the one closest to the previous step/iteration.

Validation of the algorithm

For a rigid rectangular block placed on a rigid horizontal ground [Fig. 2(a)], Shenton H. [22] obtained the relation between the horizontal ground acceleration and the coefficient of friction required to initiate the response of the block in rocking, sliding or coupled rocking-sliding mode. Shenton H. [22] used force and moment balance equations to arrive at the separatrix between the different response modes. Here, we consider an analogous problem of a rigid rectangular block impacting a rigid horizontal ground. At the instant before the impact, the block is assumed to be translating with a horizontal velocity ($\dot{u}_x > 0$) and a vertical velocity ($\dot{u}_y < 0$) in the presence of gravitational acceleration. Under the assumption that the impact between the block and ground is inelastic, i.e., $e = 0$, the block may come to rest, may start to rock, may slide, or may experience sliding coupled with rocking after the impact. Therefore, an approach similar to Shenton's method, involving conservation of linear and angular momentum, may be used to arrive at the separatrix between the different modes as a function of the translational velocities before impact ($\dot{u}_x$ and $\dot{u}_y$) and the coefficient of friction ($\mu_s = \mu_d = \mu$) between the two surfaces [Fig. 2(b)]. The details of this calculation are presented in Appendix B of [27]. For example, the separatrix between the rocking mode and the coupled rocking-sliding mode is given by:

$$ \left| \frac{\dot{u}_y}{\dot{u}_x} \right| = \frac{4 + \frac{h}{b}^2 - 3\mu\frac{h}{b}}{\mu(1 + 4\frac{h}{b}^2) - 3\frac{h}{b}} \tag{31} $$

For this analysis, the rigid block [Fig. 2(a)] considered has a half height $h = 0.6$ m, half width $b = 0.2$ m, mass $\mathrm{m} = 100$ kg, and it may only come in contact with the ground at points O_1 and O_2. The

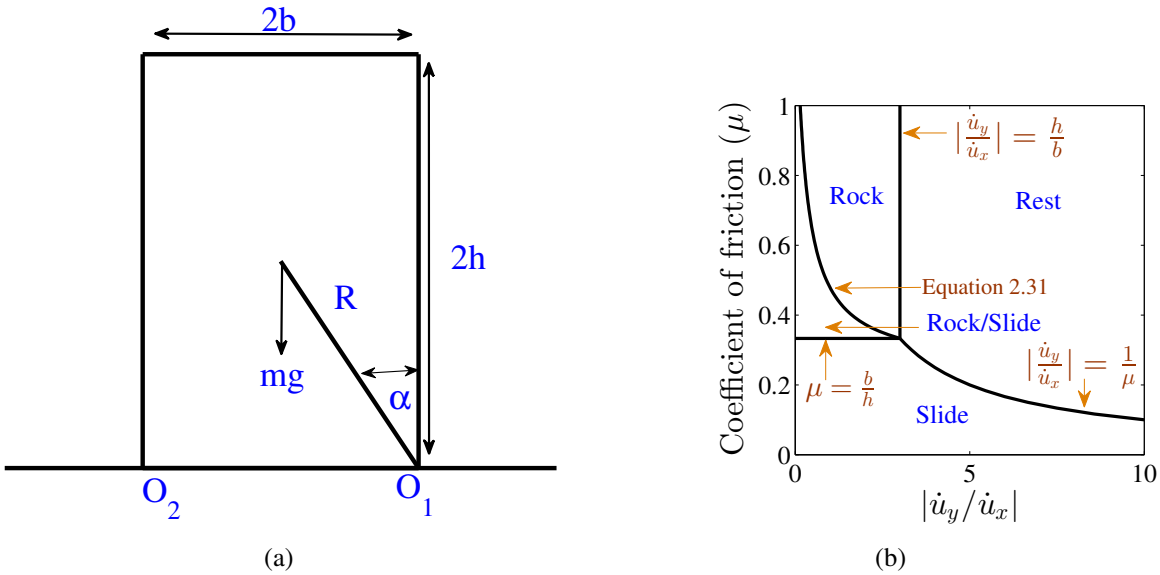

(a) (b)

Figure 2: (a) Rigid rectangular block and ground (b) motion of block after it impacts the ground as a function of initial velocity and coefficient of friction.

motion of the block after impact is governed by Lagrangian mechanics with the reduced translational and rotational velocity of the center of mass after inelastic impact as initial conditions. These velocities are also obtained by conserving angular and linear momentum as shown in Appendix B of [27]. Here, we select two combinations of $|\dot{u}_y/\dot{u}_x|$ and μ corresponding to the rocking and the coupled rocking-sliding modes and compare the solutions obtained from the rigid body dynamics algorithm with that obtained by time-integrating the equations of motion for the corresponding response modes.

The non-linear equation of motion for the rocking mode and the reduction in rotational velocity on inelastic impact during rocking was presented by Zhang and Makris (Eqs. 10 and 15 in [31]). Ishiyama worked out the nonlinear equations of motion for the coupled rocking-sliding mode (Eqs. 1-3 in [13]). These equations of motion are time integrated using the 4th order Runge Kutta method and the horizontal (x) displacement of the center of mass is compared with that obtained from the rigid body dynamics algorithm for two combinations of $|\dot{u}_y/\dot{u}_x|$ and μ corresponding to the rocking and the coupled rocking-sliding modes as shown in Figs. 3(a) and 3(b), respectively. The results using the rigid body dynamics algorithm agree very well with the analytical results.

Application

In the previous section, the response of a translating rigid rectangular block impacting a rigid ground was analyzed and it was shown that the response mode of the block after impact can be determined analytically. An extension to that study is presented in this section by analyzing a rigid rectangular block which is given an initial angular displacement or tilt θ_0 (Fig. 4) and then released. The goal is to track the response mode of the block from the time of release ($t = 0$) till the instant just after the block impacts the ground. The rectangular block and the ground are rigid and collisions between the block and ground are assumed to be perfectly inelastic (i.e., coefficient of restitution, e, is zero). Additionally, the block is assumed to come in contact with the ground only at the two corners O_1 and O_2.

As seen in the previous section, the translational and rotational velocities of the block just before impact are required to understand the response of the block just after impact. In the case of a slender block with high coefficient of friction between block and the ground, the block will only rock and will not slide on the

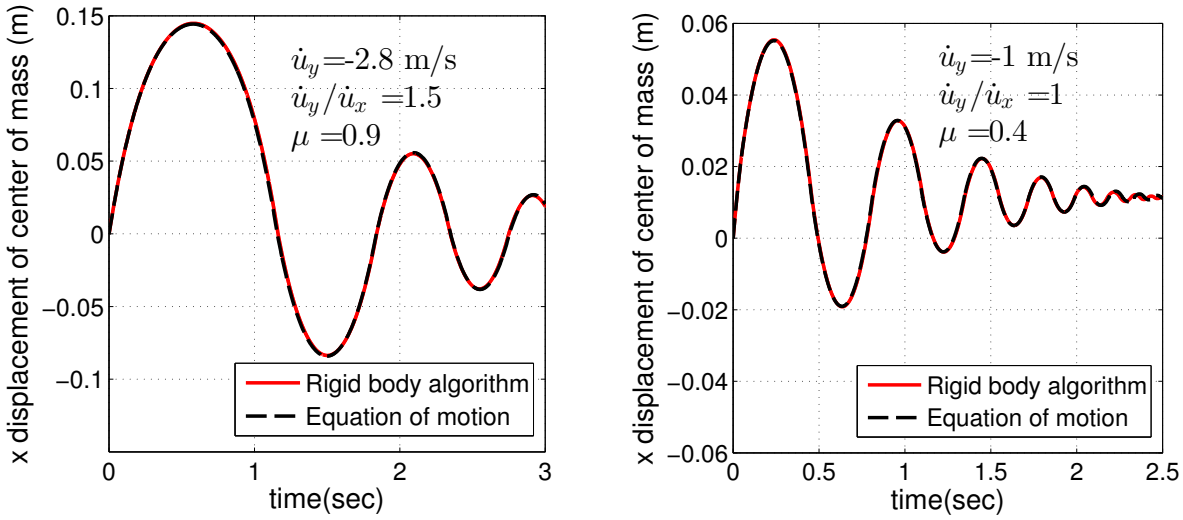

Figure 3: Comparison of x displacement time history of center of mass given by the rigid body dynamics algorithm against analytical solution for (a) rocking mode and (b) coupled rocking-sliding mode. For the rocking mode, $\dot{u}_y = -2.8$ m/s, $|\dot{u}_y/\dot{u}_y| = 1.5$ and $\mu = 0.9$. For the coupled rocking-sliding mode, $\dot{u}_y = -1$ m/s, $|\dot{u}_y/\dot{u}_y| = 1$ and $\mu = 0.4$.

ground. This scenario has been analytically studied by many scientists [12, 16, 17]. In this special case, the velocity of the block just before impact can be obtained by balancing the total energy of the block, without solving the equation of motion. However, in cases where the block is not slender or when the friction coefficient is not sufficiently high, the block may experience sliding coupled with rocking. In these cases, a part of the block's energy is dissipated by frictional forces. So, the block's velocity just before it impacts the ground cannot be estimated without solving the equations of motion. The equations of motion describing this problem are nonlinear and discontinuous and a closed form solution describing the rocking, sliding and coupled rocking-sliding response of a general rectangular block cannot be obtained even for this simple case with no external forcing. The algorithm presented this paper is well suited to analyze this complex problem.

Since the response mode of the block varies with many parameters, a comprehensive parametric study is needed to fully understand the different response modes of the rectangular block and the effect of block geometrical parameters, initial tilt angle and friction coefficient on the block's response mode. The parameters in the problem are the initial tilt angle (θ_0), friction coefficient (μ), height of the block ($2h$), width of the block ($2b$), acceleration due to gravity (g) and time but all these parameters are not necessarily required for fully describing the problem. For example, the height and width of the block can be combined to obtain the dimensionless slenderness angle ($\frac{\pi}{2} - \alpha$). Another dimensionless parameter is gT^2/b, where T is the characteristic time period for the problem. T can be obtained from moment balance about O_1 as shown below:

$$I\ddot{\theta}(t) = -mgRcos(\alpha + \theta) \implies \ddot{\theta}(t) = -\frac{3g}{4R}cos(\alpha + \theta) = -\frac{1}{T^2}cos(\alpha + \theta) \tag{32}$$

where, $I = \frac{4}{3}mR^2$ is the second moment of area of the block about corner O_1, m is the mass of the block, and $\ddot{\theta}(t)$ is the block's angular acceleration at time t. Using the value of $T = \sqrt{4R/3g}$ from Eq. 32, the dimensionless parameter gT^2/b becomes $4R/3b = 4/3sec(\alpha)$ and is therefore not an independent parameter. So, the three independent dimensionless parameters that fully describe the problem and hence used in this parametric study are θ_0, μ and α.

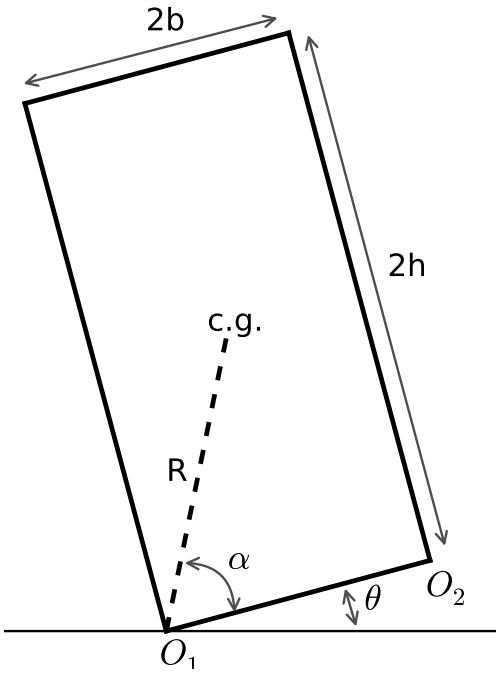

Figure 4: Initial configuration of the rectangular block with an angular displacement or tilt of θ_0 with respect to the ground.

The parameters α and θ_0 are varied from 5° to 75° and 10° to $85^\circ - \alpha$, respectively, in steps of 5°. The maximum limit for θ_0 is chosen to be $85^\circ - \alpha$ because: (i) when $\theta_0 = 90^\circ - \alpha$, the center of mass of the block is vertically aligned with the point of contact (O_1), placing the block in an unstable equilibrium from which it will not move until perturbed, and (ii) when $\theta_0 > 90^\circ - \alpha$, the block will overturn as the moment due to it's weight is no longer a stabilizing factor. The last parameter μ is varied from 0.1 to 1.5 in steps of 0.1. In total, 1800 scenarios are simulated using the rigid body dynamics algorithm.

The vertical position and horizontal velocity time histories of the two corners (O_1 and O_2) are calculated for each scenario. If the absolute vertical position of a corner is within 0.0001 m (contact tolerance) of the rigid ground, the corner is said to be in contact with the ground. If a corner is in contact with the ground and if its horizontal velocity is greater than 0.0001 m/s (sliding tolerance), the corner is said to be sliding with respect to the ground. The velocity and displacement time histories of O_1 (solid red line) and O_2 (dashed black line) for 4 different parameter combinations are shown in Fig. 5.

Let t_i be the time of impact, i.e., the time at which the corner O_2 comes into contact with the ground. The problem can be divided into two cases, time of release to the instant just before impact ($0 \leq t < t_i$) and the time instant just after impact ($t = t_i^+$).

Case I: $0 \leq t < t_i$

This case examines the response of the block from the time it is released to the time instant just before impact (t_i^-). During this time interval, O_1 is in contact with the ground and O_2 is not in contact with the ground. The only two possible response modes of the block during this time interval are (i) pure rocking, and (ii) combined rocking and sliding. If the horizontal velocity of O_1 is greater than sliding tolerance for any $t \in [0, t_i)$, then the block is sliding as well as rocking, else the block is exhibiting pure rocking response. In Fig. 5(a), the block is exhibiting combined rocking and sliding mode as the horizontal velocity of O_1 (solid red line) is non-zero before impact (which occurs around 0.58 s). In Figs. 5(b)-5(d), the block is exhibiting pure rocking response mode before impact. Figure 6 shows the response mode of the block as a function

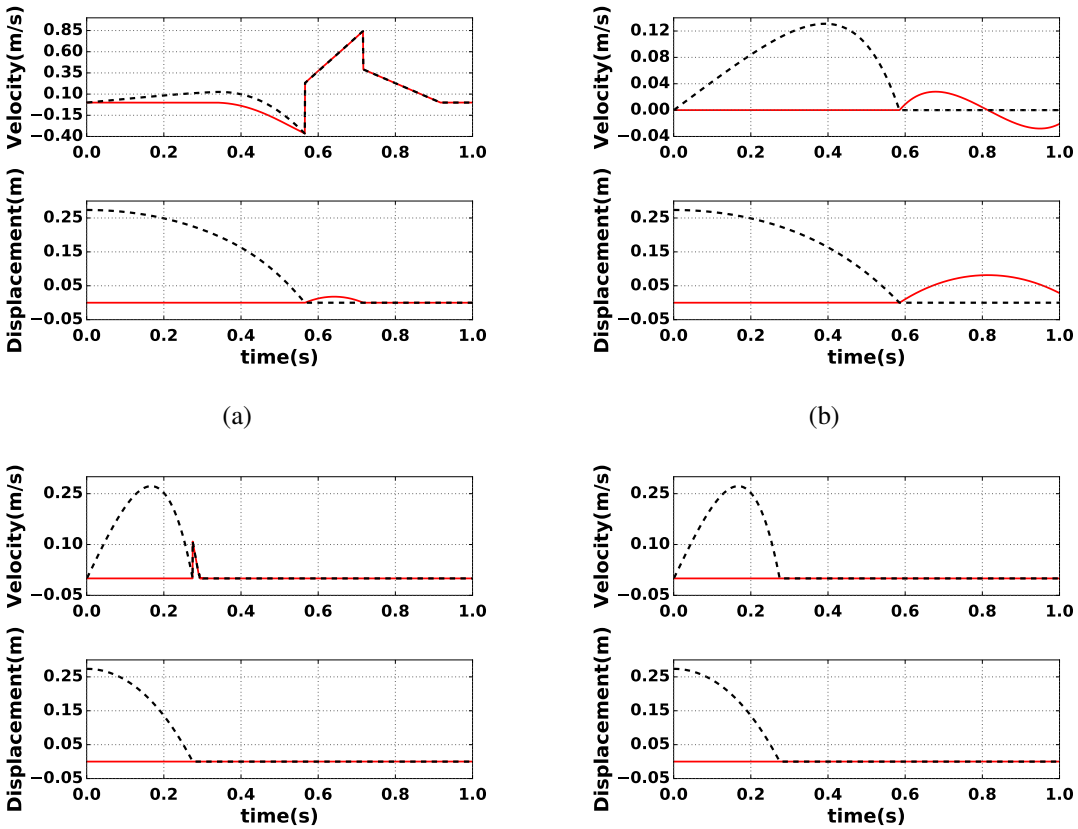

Figure 5: Horizontal velocity and vertical position time histories for the two corners O_1 (solid red line) and O_2 (dashed black line) for (a) $\alpha = 60^\circ$, $\theta_0 = 20^\circ$ and $\mu = 0.2$ (rock+slide before impact to rock+slide after impact), (b) $\alpha = 60^\circ$, $\theta_0 = 20^\circ$ and $\mu = 0.8$ (pure rock before impact to pure rock after impact), (c) $\alpha = 35^\circ$, $\theta_0 = 20^\circ$ and $\mu = 0.6$ (pure rock before impact to slide after impact), and(d) $\alpha = 35^\circ$, $\theta_0 = 20^\circ$ and $\mu = 0.8$ (pure rock before impact to rest after impact) .

of α and μ for different values of θ_0. The green and blue rectangles in these figures are the parameter combinations for which the block exhibits pure rocking and combined rocking and sliding response before t_i, respectively. These figures show that a slender block (i.e, higher alpha) is more likely to rock for a fixed μ than a stouter block. Also, for a fixed α, the block is more likely to exhibit combined rocking and sliding at lower values of μ and pure rocking at higher values of μ.

The transition from pure rocking to combined rocking and sliding in the $\alpha - \mu$ space changes with the initial displacement θ_0, which is a measure of the potential energy imparted to the block. For blocks with $\alpha > 45^\circ$, a higher θ_0 causes the block to exhibit pure rocking at lower values of μ, while the effect is reversed for stouter blocks. For example, the block exhibits combined sliding and rocking at $\alpha = 50^\circ$ and $\mu = 0.4$ for $\theta_0 = 10^\circ$ [Fig. 6(a)], whereas it has transitioned to pure rocking mode at the same α and μ for $\theta_0 = 30^\circ$ [Fig. 6(c)]. The reverse effect is seen at $\alpha = 30^\circ$ and $\mu = 0.7$ where the block is exhibiting pure rocking response for $\theta_0 = 10^\circ$ [Fig. 6(a)] and combined rocking and sliding mode for $\theta_0 = 30^\circ$ [Fig. 6(c)].

To get a clearer understanding of these results, an analytical expression describing the minimum μ required to sustain pure rocking response before t_i is obtained using force and moment balance equations. Let $\theta(t)$ be the angular displacement of the block such that $\theta(0) = \theta_0$. Then $\dot{\theta}(t)$ and $\ddot{\theta}(t)$ are the angular velocity and acceleration of the block, respectively. Note that counter clock wise rotation is considered

positive. Then, moment balance about O_1 and force balance gives:

$$I\ddot{\theta}(t) = -mgRcos(\alpha+\theta) \implies \ddot{\theta}(t) = -\frac{3g}{4R}cos(\alpha+\theta) \tag{33}$$

$$f_x = m\ddot{x}(t) \tag{34}$$

$$f_y - mg = m\ddot{y}(t) \tag{35}$$

where $I = \frac{4}{3}mR^2$ is the second moment of area of the block about corner O_1, m is the mass of the block, g is the acceleration due to gravity, $\ddot{x}(t)$ and $\ddot{y}(t)$ are the horizontal and vertical accelerations of the center of mass, respectively, and f_x and f_y are the frictional and normal contact forces at O_1, respectively.

Since $\ddot{\theta}(t) = d\dot{\theta}(t)/dt$ and $\dot{\theta}(t) = d\theta(t)/dt$, Eq. 33 can be rewritten as:

$$\int_0^{\dot{\theta}(t)} \dot{\theta}d\dot{\theta} = \int_{\theta_0}^{\theta(t)} -\frac{3g}{4R}cos(\alpha+\theta)d\theta \implies \dot{\theta}^2(t) = \frac{3g}{2R}[sin(\alpha+\theta_0) - sin(\alpha+\theta(t))] \tag{36}$$

The pure rocking response of the block about corner O_1 implies that the horizontal and vertical accelerations of O_1 are zero at any time $t \in [0, t_i)$. This gives:

$$\ddot{x}(t) = -\ddot{\theta}(t)Rsin(\alpha+\theta(t)) - \dot{\theta}^2(t)Rcos(\alpha+\theta(t))$$

$$\ddot{y}(t) = \ddot{\theta}(t)Rcos(\alpha+\theta(t)) - \dot{\theta}^2(t)Rsin(\alpha+\theta(t))$$

Substituting the above values of $\ddot{x}(t)$ and $\ddot{y}(t)$ into Eqs. 34 and 35, respectively, and using the expressions for $\ddot{\theta}(t)$ and $\dot{\theta}(t)$ from Eqs. 33 and 36, respectively, f_x and f_y can be estimated in terms of α, $\theta(t)$, θ_0 and g. Finally, since the point O_1 is not sliding with respect to the ground, $\|f_x\| \leq \mu f_y$ from Coulomb's laws of friction. This implies:

$$\frac{\|[3sin(\alpha+\theta(t)) - 2sin(\alpha+\theta_0)]cos(\alpha+\theta(t))\|}{[3sin(\alpha+\theta(t)) - 2sin(\alpha+\theta_0)]sin(\alpha+\theta(t)) + 1/3} \leq \mu \tag{37}$$

The above expression provides the minimum μ required to sustain pure rocking mode of the block before t_i. The left hand side of the above equation contains time varying angular displacement, i.e., $\theta(t)$, resulting in a time (or θ) varying minimum μ. The maximum value of the expression to the left of the inequality for $0 \leq t < t_i$ (or equivalently $\theta_0 \geq \theta(t) > 0$) gives the minimum μ required to sustain pure rocking mode of the block for $t \in [0, t_i)$. The resulting minimum μ as a function of α and θ_0 is plotted in Fig. 6 using the black solid line. In each figure, for any $\alpha - \mu$ combination above the black line, the block will exhibit pure rocking mode for any $t \in [0, t_i)$, and for any $\alpha - \mu$ combination below the black line, it will exhibit combined rocking and sliding response mode atleast for some finite time interval in $[0, t_i)$. These figures show that the results obtained from the rigid body algorithm agree well with the analytical solution.

A key point to note in the above analysis is that the block's response mode is classified as 'combined rocking and sliding' if the horizontal velocity of O_1 is greater than the sliding tolerance for any finite time interval between $[0, t_i)$. Is it possible that a block that starts to exhibit combined rocking and sliding , say at $t_s \in [0, t_i)$, changes its mode back to pure rocking before t_i? To answer this question, the horizontal velocity of O_1 for $t \in [t_s, t_i)$ is analyzed. If the horizontal velocity in the considered time interval becomes less than the sliding tolerance for a finite time interval, it implies that the response mode of the rock has changed from combined rocking and sliding to pure rocking. Considering a finite time interval (2 time steps or more) is required because in certain cases the horizontal velocity of O_1 transitions from negative to positive velocity in $t \in [t_s, t_i)$. During this transition, the horizontal velocity may be less than the sliding tolerance at a particular time instant, leading to an erroneous classification of the mode begin changed from combined rocking and sliding to pure rocking. Another method to verify the correct classification of this mode change is to assert that the horizontal acceleration is zero (within a tolerance) at the time instant when horizontal velocity is less than the sliding tolerance. Analyzing the horizontal velocity and acceleration of O_1 for all the cases that experienced combined rocking and sliding response shows that there was no mode changes from combined rocking and sliding to pure rocking between t_s and t_i implying that a block that starts sliding coupled with rocking, continues in the same mode until the time of impact t_i.

Case II: $t = t_i^+$

Next, the response of the block just after impact is analyzed. Here, O_2 is in contact with the ground, i.e., vertical displacement of O_2 is less than contact tolerance. As seen in the previous section, the block can exhibit four different response modes after impact with the ground : pure rocking, combined rocking and sliding, pure sliding or the block can come to rest. If O_1 is no longer in contact with the ground after impact and if the horizontal velocity of O_2 is less than sliding tolerance, then the block is purely rocking about O_2 [Fig. 5(b)]. On the other hand, if O_1 is not in contact but horizontal velocity of O_2 is greater than sliding tolerance, then block is experiencing rocking coupled with sliding after impact [Fig. 5(a)]. If both O_1 and O_2 are in contact with the ground and the horizontal velocity of O_2 is greater than sliding tolerance, then the block is sliding on the ground [Fig. 5(c)]. Else the block has come to rest [Fig. 5(d)].

Fig. 7 shows the response modes of the block just before and just after impact as a function of α and μ for different initial tilt θ_0. The response mode of the block before impact is given by the solid black line with all parameter combinations above this line indicating pure rocking response before impact and those below indicating combined sliding and rocking response before impact. The response modes of the block after impact are given by the rectangles. Grey, yellow and blue rectangles indicate that the block is exhibiting pure rocking, combined rocking and sliding, and pure sliding response mode, respectively, after impact with the ground. The red rectangle indicates that the block has come to rest after impact.

These figures show that pure rocking or combined rocking and sliding mode after impact does not occur for $\alpha < 35^\circ$. This criterion on α for the response mode transition from pure rocking mode before impact to pure rocking mode after impact can be demonstrated analytically by conserving the angular momentum of the block about O_2 before and after impact, i.e.,

$$I\dot{\theta}^+ = (I - 2mb^2)\dot{\theta}^-$$

where $\dot{\theta}^-$ and $\dot{\theta}^+$ are the angular velocities of the block before and after impact, respectively, and $I = 4/3mR^2$ is the second moment of the area of the block about O_2. Since the angular velocity should be of the same sign before and after impact:

$$I - 2mb^2 \geq 0 \implies \frac{4}{3}(b^2 + h^2) \geq 2b^2 \implies \frac{h}{b} \geq \frac{1}{\sqrt{2}}$$
$$\implies \alpha \geq 35.26^\circ$$

Fig. 7 also shows that for $\alpha > 30^\circ$, if the block was exhibiting combined rocking and sliding before impact, it exhibits either pure sliding or combined rocking and sliding response after impact as well. However, the reverse is not always true, i.e., if the block was exhibiting pure rocking response before impact, then in a few of these cases the block exhibits combined rocking and sliding or pure sliding response after impact. These outlier cases can be seen near the solid black line. For example, for $\alpha = 40^\circ$, $\theta_0 = 30^\circ$ and $\mu = 0.5$ and $\mu = 0.6$ [Fig. 7(c)], the block experienced pure rocking response before impact and pure sliding and combined rocking and sliding response, respectively, after impact.

Another interesting result from Fig. 7(a)-7(d) is that the stouter blocks ($\alpha \leq 30^\circ$) come to rest after impact for $\theta_0 \leq 40^\circ$ implying that all the energy of the block is dissipated during the impact. This limit on α below which the block comes to rest decreases with increase in θ_0 [Figs. 7(e)-7(f)] indicating that when a higher potential energy is imparted to the block (by increasing θ_0), even the stouter blocks with $\alpha < 30^\circ$ has sufficient energy to slide after impact. The role played by θ_0 in changing the response mode of the block after impact becomes apparent only in Figs. 7(e)-7(f). The response mode exhibited by the block after impact is remarkably similar in Figs. 7(a)-7(d) even though the response mode before impact were quite different in all four cases. The results presented in this section demonstrate the usefulness of this algorithm in numerically solving complex rigid body dynamics problems where multiple response modes are present.

Conclusion

In this paper, a rigid body dynamics algorithm is presented to accurately model the 3-D rocking and/or sliding response of a rigid body when the ground underneath it is subjected to earthquake excitation. The algorithm picks the closest solution for the contact forces/impulses at each iteration/step thus eliminating the ambiguity resulting from the presence of infinite mathematically admissible solutions.

This algorithm is validated against analytical results for the rocking and coupled rocking-sliding response of a 2-D rectangular block. This validated algorithm is then used to model the response of a rectangular block which is given an initial tilt and then released. The response of this block is sensitive to the slenderness angle, friction coefficient between the block and the ground and the initial tilt. Before impact with the ground, a slender block with higher friction coefficient exhibits pure rocking response mode while a stouter block with lower friction coefficient exhibits coupled rocking-sliding response mode. Once the response mode of the block enters the coupled rocking-sliding mode, this mode is preserved until the block impacts the ground.

Once the block impacts the ground, it can respond in 4 different modes. It can exhibit pure rocking or coupled rocking-sliding or pure sliding response mode or it can come to rest. This analysis showed that: (i) if the block exhibits coupled rocking-sliding response before impact, it exhibits coupled rocking-sliding or pure sliding response after impact as well. However, coupled rocking-sliding before impact is not a necessary condition for pure sliding or coupled rocking-sliding after impact. (ii) A minimum slenderness criteria has to be satisfied ($\alpha > 35^\circ$) for the block to exhibit pure rocking or coupled rocking-sliding response after impact. (iii) The response mode of a stouter block depends on the potential energy imparted to the block (or equivalently initial tilt angle) and the friction coefficient of the block. A stouter block ($\alpha < 30^\circ$) comes to rest after impact for moderate initial tilt angles ($10^\circ \leq \theta_0 \leq 40^\circ$) while it slides after impact for higher tilt angles ($\theta_0 > 40^\circ$) and lower friction coefficients.

In addition to this class of problems, the algorithm may be used to simulate the rocking and sliding response of precariously balanced rocks under earthquake excitation to place upper bounds on historical shaking in the region [28]. It may also be extended to model the response of multi-body systems such as the stacked column structures found in Greece [18] and linked structures such as robotic arms.

Appendix

In this appendix, we prove that the LCP in Eq. 16 is feasible, i.e., there exists a ${\mathbf{j_n}}^{p+1}$ satisfying all the inequality constraints. Say, the normal vector $\boldsymbol{n_\alpha}$ (size 1×3) at all contact points ($\alpha = 1, 2, .., q$) are arranged into the matrix $\mathbf{J}$ of size $q \times 3$. Similarly, say the row vectors $\boldsymbol{r_\alpha} \times \boldsymbol{n_\alpha}$ (size 1×3) at all contact points are arranged into the matrix $\mathbf{K}$. Then, from the definition of the $\mathbf{C_{nn}}$ in Eq. 15, $\mathbf{C_{nn}}$ can be rewritten as:

$$\mathbf{C_{nn}} = \frac{1}{m}\mathbf{J}\mathbf{J}^T + \mathbf{K}\mathbf{I}^{-1}\mathbf{K}^T \tag{38}$$

Now, from Farkas's alternative [11], either there exists a non-negative ${\mathbf{j_n}}^{p+1}$ satisfying ${\mathbf{j_n}}^{p+1}\mathbf{C_{nn}} + \mathbf{d'_n} \geq \mathbf{0}$, or there exists a positive row vector $\mathbf{h}$ (size $1 \times q$) satisfying $-\mathbf{h}\mathbf{C_{nn}} \geq \mathbf{0}$ and $\mathbf{h} \cdot \mathbf{d'_n} < \mathbf{0}$ (where $\cdot$ represents element-wise multiplication). Say there exists a $\mathbf{h}$ meeting the specified requirements. Since $\mathbf{h}$ is a positive vector, $-\mathbf{h}\mathbf{C_{nn}}\mathbf{h}^T \geq 0$. However, $\mathbf{C_{nn}}$ is positive semi-definite. Therefore, $\mathbf{h}\mathbf{C_{nn}}\mathbf{h}^T = 0$. Now substituting for $\mathbf{C_{nn}}$ from Eq. 38, we get:

$$\begin{aligned}
\mathbf{h}\mathbf{C_{nn}}\mathbf{h}^T = 0 &\implies \mathbf{h}(\frac{1}{m}\mathbf{J}\mathbf{J}^T + \mathbf{K}\mathbf{I}^{-1}\mathbf{K}^T)\mathbf{h}^T = 0 \\
&\implies \frac{1}{m}\mathbf{h}\mathbf{J}\mathbf{J}^T\mathbf{h}^T + \mathbf{h}\mathbf{K}\mathbf{I}^{-1}\mathbf{K}^T\mathbf{h}^T = 0 \\
&\implies \frac{1}{m}\|\mathbf{J}^T\mathbf{h}^T\|^2 + (\mathbf{K}^T\mathbf{h}^T)^T\mathbf{I}^{-1}(\mathbf{K}^T\mathbf{h}^T) = 0
\end{aligned}$$

Since moment of inertia, $\mathbf{I}$, is positive definite:

$$\mathbf{h}\mathbf{C_{nn}}\mathbf{h}^T = 0 \implies \mathbf{J}^T\mathbf{h}^T = \mathbf{0}; \quad \mathbf{K}^T\mathbf{h}^T = \mathbf{0}$$

From the definition of $\mathbf{J}$,

$$\mathbf{J}^T\mathbf{h}^T = \mathbf{0} \implies \sum_{\alpha=1}^{q} \boldsymbol{n_\alpha}^T h_\alpha = \mathbf{0}$$

Here, h_α is the α^{th} element of the vector $\mathbf{h}$. In the types of problems we are considering, the vertical component (i.e., global Z) of the outward normal vector to the pedestal surface at all contact points is positive. Since $\mathbf{h}$ is also a positive vector, $\sum_{\alpha=1}^{q} \boldsymbol{n_\alpha}^T h_\alpha$ can never be zero. Therefore, a positive vector $\mathbf{h}$ (size $1 \times q$) satisfying $-\mathbf{h}\mathbf{C_{nn}} \geq \mathbf{0}$ and $\mathbf{h} \cdot \mathbf{d'_n} < \mathbf{0}$ does not exist. The non-existence of $\mathbf{h}$ mandates the existence of a non-negative $\mathbf{j_n}^{p+1}$ satisfying $\mathbf{j_n}^{p+1}\mathbf{C_{nn}} + \mathbf{d'_n} \geq \mathbf{0}$, thereby ensuring the feasibility of the LCP.

References

[1] D. Baraff. Non-penetrating rigid body simulation. In *State of the Art Reports, Eurographics '93*, 1993.

[2] D. Baraff. Fast contact force computation for nonpenetrating rigid bodies. In *Computer Graphics Proceedings(SIGGRAPH)*, 1994.

[3] J. Bender, D. Finkenzeller, and A. Schmitt. An impulse-based dynamic simulation system for VR applications. *In Proceedings of Virtual Concept 2005(Biarritz, France, 2005), Springer*, 2005.

[4] J. Bender and A. Schmitt. Constraint-based collision and contact handling using impulses. *In Proceedings of the 19th international conference on computer animation and social agents (Geneva (Switzerland)*, pages 3–11, 2006.

[5] A. Cayley. Sur quelques proriétés des déterminants gauches. *Journal für die Reine und Angewandte Mathematik*, 32:119–123, 1846.

[6] M. N. Chatzis and A. W. Smyth. Modeling of the 3D rocking problem. *Journal of Non-Linear Mechanics*, 47(4):85–98, 2012.

[7] M. N. Chatzis and A. W. Smyth. Three-dimensional dynamics of a rigid body with wheels on a moving base. *Journal of Engineering Mechanics*, 139(4):496–511, 2013.

[8] R.W. Cottle and G.B. Dantzig. *Complementary pivot theory of mathematical programming*. 1968.

[9] R.W. Cottle, J.S. Pang, and R.E. Stone. *The Linear Complementarity Problem*. 1992.

[10] Cyberbotics. Webots 6. *http://www/cyberbotics.com/webbots*, 2009.

[11] G. Farkas. Über die theorie der einfachen ungleichungen. *Journal für die Reine und Angewandte Mathematik*, 124:1–27, 1902.

[12] G. W. Housner. The behavior of inverted pendulum structures during earthquakes. *Bulletin of the Seismological Society of America*, 53(2):403–417, 1963.

[13] Y. Ishiyama. Motions of rigid bodies and criteria for overturning by earthquake exictations. *Earthquake Engineering and Structural Dynamics*, 10:635–650, 1982.

[14] S. G. Johnson. The NLopt nonlinear-optimization package. *http://ab-initio.mit.edu/nlopt*.

[15] N. Kikuchi and J. Oden. Contact problems in elasticity: A study of variational inequalities and finite element methods. 1988.

[16] T.R. Kimura and K. Iida. On the rocking of rectangular columns (I). *Zisin*, 6(3):125–149, 1934.

[17] P. Kirkpatrick. Seismic measurements by the overthrow of columns. *Bulletin of Seismological Society of America*, 17(2):95–109, 1927.

[18] A.N. Kounadis. On the rocking complex response of ancient multispondyle columns: A genious and challenging structural system requiring reliable solution. *Meccanica*, 2014.

[19] D. Kraft. Algorithm 733: TOMP-Fortran modules for optimal control calculations. *ACM Transactions on Mathematical Software*, 20(3):262–281, 1994.

[20] P. Lötstedt. Numerical simulation of time-dependent contact and friction problems in rigid body mechanics. *SIAM Journal on Scientific and Statistical Computing*, 5(2):370–393, 1984.

[21] Microsoft. Microsoft robotics. *http://www/microsoft.com/robotics*, 2009.

[22] H.W. Shenton. Criteria for initiation of slide, rock, and slide-rock rigid-body modes. *Journal of Engineering Mechanics*, 122:690–693, 1996.

[23] R. Smith. Open Dynamics Engine. *http://www/ode.org*, 2000.

[24] D.E. Stewart and J.C. Trinkle. An implicit timestepping scheme for rigid body dynamics with inelastic collisions and Coulomb friction. *International Journal of Numerical Methods in Engineering*, 1996.

[25] E. Stoneking. Newton-Euler dynamic equations of motion for a multi-body spacecraft. *AIAA Guidance, Navigation, and Controil Conference*, pages 1368–1380, 2007.

[26] B. Sweetman and L. Wang. Floating offshore wind turbine dynamics: Large-angle motions in Euler space. *Journal of Offshore Mechanics Architecture Engineering*, 134(3), 2012.

[27] S. Veeraraghavan. *Toppling analysis of precariously balanced rocks*. PhD thesis, California Institute of Technology, 2015.

[28] S. Veeraraghavan, K. Hudnut, and S. Krishnan. Toppling analysis of the Echo Cliffs precariously balanced rock. *Bulletin of the Seismological Society of America*, 107(1), 2017.

[29] E. Voyagaki, L. N. Psycharis, and G. Mylonakis. Complex response of a rocking block to a full-cycle pulse. *Journal of Engineering Mechanics*, 140(6):1071–1083, 2014.

[30] R. Weinstein, J. Teran, and R. Fedkiw. Dynamic simulation of articulated rigid bodies with contact and collision. *IEEE Transactions on Visualization and Computer Graphics*, 12(3):365–374, 2006.

[31] J. Zhang and N. Makris. Rocking response of free-standing blocks under cycloidal pulses. *Journal of Engineering Mechanics*, 127:473–483, 2001.

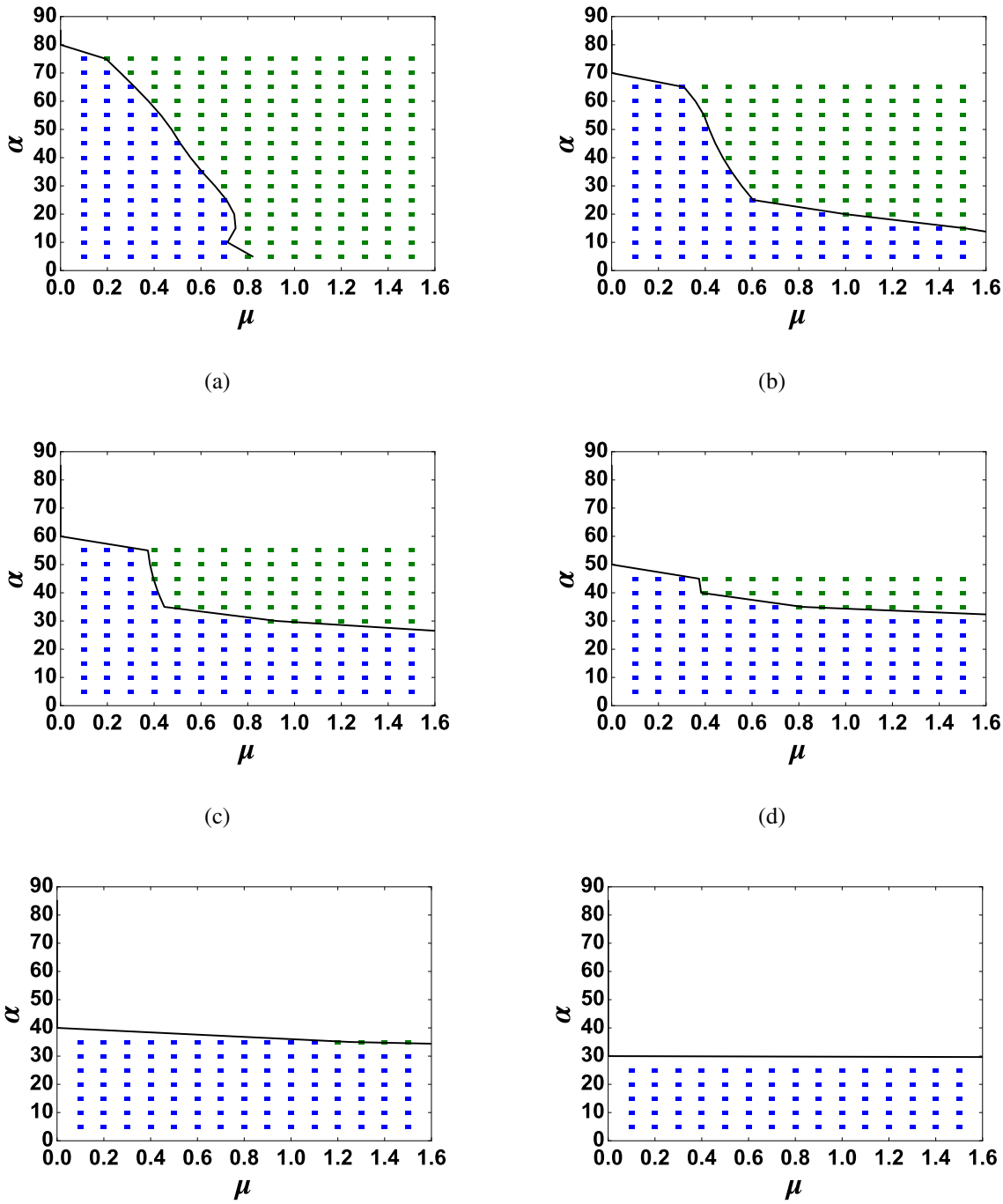

Figure 6: Response mode of the block for initial angular displacement of (a) 10°, (b) 20°, (c) 30°, (d) 40°, (e) 50° and (f) 60°. Blue rectangle indicates rocking coupled with sliding, and green rectangle indicates pure rocking response of the block before impact. The solid black line is the minimum friction required for pure rocking response of the block from Eq. 37. The block exhibits pure rocking response for the parameter combinations to the right of the solid black line and exhibits coupled rocking-sliding response for those below the line.

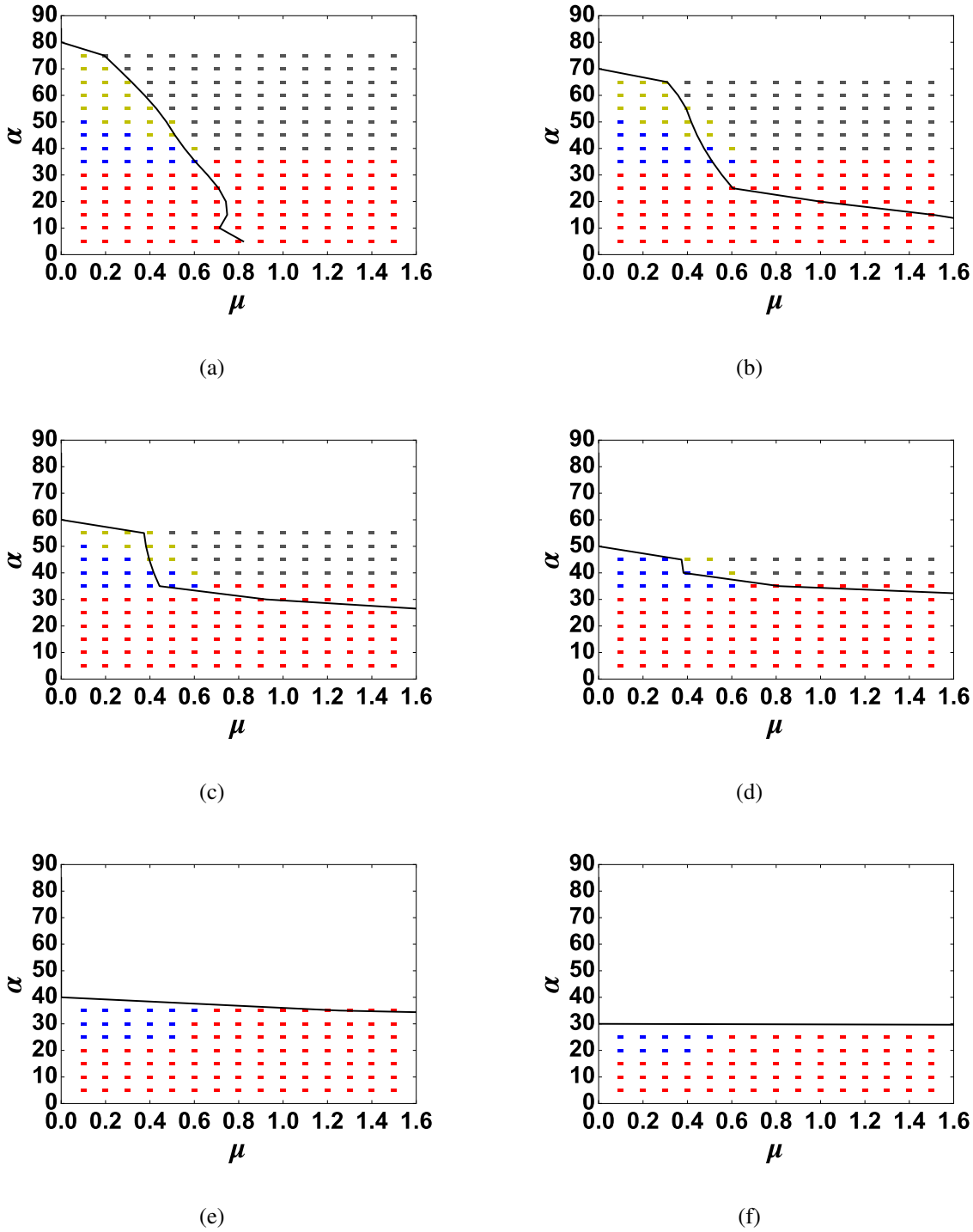

Figure 7: Response mode of the block before and after block impacts the ground for initial angular displacement of (a) 10°, (b) 20°, (c) 30°, (d) 40°, (e) 50° and (f) 60°. The parameter combinations to the right of the solid black line indicates pure rocking response before impact and those below the line indicates coupled rocking-sliding response before impact. Yellow, grey and blue rectangles indicate that the block is exhibiting coupled rocking-sliding, pure rocking and pure sliding response after impact with the ground. The red rectangles indicate that the block comes to rest after impact with the ground.